1   # Mechanisms of dissolved and labile particulate iron supply to shelf

2   # waters and phytoplankton blooms off South Georgia, Southern Ocean

3   Christian Schlosser[1,2,*], Katrin Schmidt[3,4], Alfred Aquilina[1], William B. Homoky[1,5], Maxi

4   Castrillejo[1,6], Rachel A. Mills[1], Matthew D. Patey[1], Sophie Fielding[3], Angus Atkinson[7], and

5   Eric P. Achterberg[1,2]

6

7   [1] Ocean and Earth Science, National Oceanography Centre Southampton, University of

8   Southampton, SO14 3ZH Southampton, United Kingdom

9   [2] GEOMAR Helmholtz Centre for Ocean Research, Wischhofstr. 1-3, 24148 Kiel, Germany

10   [3] British Antarctic Survey, CB3 0ET Cambridge, United Kingdom

11   [4] School of Geography, Earth and Environmental Sciences, University of Plymouth, PL4

12   8AA Plymouth, United Kingdom

13   [5] Department of Earth Sciences, University of Oxford, OX1 3AN Oxford, United Kingdom

14   [6] Institut de Ciència i Tecnologia Ambientals & Departament de Física, Universitat

15   Autònoma de Barcelona, 08193 Bellaterra, Spain

16   [7] Plymouth Marine Laboratory, Prospect Place, The Hoe, PL1 3DH Plymouth, United

17   Kingdom

18

19

20   For submission to Biogeosciences

21

22   * Corresponding author Christian Schlosser (Email: cschlosser@geomar.de,

23   Phone: 0049 (0) 431 600 1297)

Abstract (375 words)

The island of South Georgia is situated in the iron (Fe) depleted Antarctic Circumpolar Current of the Southern Ocean. Iron emanating from its shelf system fuels large phytoplankton blooms downstream of the island, but the actual supply mechanisms are unclear. To address this, we present an inventory of Fe, manganese (Mn) and aluminium (Al) in shelf sediments, pore waters and the water column in the vicinity of South Georgia, alongside data on zooplankton-mediated Fe cycling processes, and provide estimates of the relative dissolved Fe (DFe) fluxes from these sources. Seafloor sediments, modified by authigenic Fe precipitation, were the main particulate Fe source to shelf bottom waters as indicated by the similar Fe/Mn and Fe/Al ratios for shelf sediments and suspended particles in the water column. Less than 1% of the total particulate Fe pool was leachable surface adsorbed (labile) Fe, and therefore potentially available to organisms. Pore waters formed the primary DFe source to shelf bottom waters supplying $0.1 - 44$ µmol DFe m^{-2} d^{-1}. However, we estimate that only 0.41 ± 0.26 µmol DFe m^{-2} d^{-1} was transferred to the surface mixed layer by vertical diffusive and advective mixing. Other trace metal sources to surface waters included glacial flour released by melting glaciers and via zooplankton egestion and excretion processes. On average 6.5 ± 8.2 µmol m^{-2} d^{-1} of labile particulate Fe was supplied to the surface mixed layer via faecal pellets formed by Antarctic krill (*Euphausia superba*), with a further 1.1 ± 2.2 µmol DFe m^{-2} d^{-1} released directly by the krill. The faecal pellets released by krill included seafloor-derived lithogenic and authigenic material and settled algal debris, in addition to freshly ingested suspended phytoplankton cells.

The Fe requirement of the phytoplankton blooms ~1,250 km downstream of South Georgia was estimated at 0.33 ± 0.11 µmol m^{-2} d^{-1}, with the DFe supply by horizontal/vertical mixing, deep winter mixing and aeolian dust estimated as ~0.12 µmol m^{-2} d^{-1}. We hypothesize that a substantial contribution of DFe was provided through recycling of

49   biogenically stored Fe following luxury Fe uptake by phytoplankton on the Fe-rich shelf.

50   This process would allow Fe to be retained in the surface mixed layer of waters downstream

51   of South Georgia through continuous recycling and biological uptake, supplying the large

52   downstream phytoplankton blooms.

1. Introduction

The Southern Ocean is the largest 'High Nitrate Low Chlorophyll' (HNLC) region of the global ocean (Buesseler et al., 2004), as a consequence of low iron (Fe) supply and subsequent reduced phytoplankton growth (Buesseler et al., 2004; Tsuda et al., 2009). Iron can be supplied to surface waters of the Southern Ocean by atmospheric dust inputs (Cassar et al., 2007; Gao et al., 2001), horizontal/vertical advective and diffusive mixing processes (de Jong et al., 2012), resuspension from shelf sediments (Kalnejais et al., 2010; Marsay et al., 2014), melting of icebergs and glaciers (Raiswell et al., 2008), and hydrothermal inputs (German et al., 2016). Despite the overall HNLC status of the Southern Ocean, regions in the wake of islands feature large seasonal phytoplankton blooms; the Fe sources to these blooms are however poorly constrained (de Jong et al., 2012; Planquette et al., 2007; Pollard et al., 2009).

Downstream of the island of South Georgia intense, long-lasting phytoplankton blooms have been observed which extend hundreds of kilometres, and require an enhanced Fe supply. The blooms peak in austral summer (Borrione et al., 2013), stretch over an area of ~ 750,000 km^2 (Atkinson et al., 2001; Korb et al., 2004), and are responsible for the largest dissolved inorganic carbon deficit reported within the Antarctic Circumpolar Current (ACC) (Jones et al., 2015; Jones et al., 2012). As a consequence of the Fe fertilisation, the waters in the vicinity of South Georgia support extensive phytoplankton blooms and a large biomass of zooplankton, fish, seabirds and marine mammals, some of which are exploited commercially (Atkinson et al., 2001; Murphy et al., 2007).

South Georgia forms part of the volcanically active Scotia Arc in the Atlantic sector of the Southern Ocean and is surrounded by a broad 30 to 100 km wide shelf with an average (albeit highly variable) depth of ca. 200 m (Fig. 1). The island is situated between the Antarctic Polar Front (PF) and the Southern ACC Front (SACCF), within the general

northeast flow of the ACC (Meredith et al., 2005; Whitehouse et al., 2008). The ACC surface waters are enriched in nitrate, phosphate and silicic acid, but strongly depleted in most trace elements, notably Fe and manganese (Mn) (Browning et al., 2014). The large seasonal phytoplankton blooms downstream of South Georgia are thought to be supplied with Fe from the island during the passage of ACC waters (Borrione et al., 2013; Nielsdóttir et al., 2012).

In this study we provide the first comprehensive data set of dissolved and (labile) particulate Fe, Mn, and Al in sediments, pore waters, and the water column overlaying the shelf and shelf edge regions of South Georgia. We also include published data on the role of Antarctic krill in new Fe supply and recycling in this region (Schmidt et al., 2011; Schmidt et al., 2016). We discuss differences between the various analysed trace metal fractions and the supply routes of dissolved and (labile) particulate Fe, such as sedimentary pore water efflux, supply of sediment derived particulate Fe to the surface mixed layer, efflux of Fe from glacial melting and supply of Fe by faecal pellets of Antarctic krill. Furthermore, we discuss the productivity of the bloom region to the north of South Georgia in relation to the estimated Fe supply rates.

2. Methods

2.1 Cruises and Sampling

Samples were collected during three research cruises to South Georgia in 2011 (JR247, JC055), and 2013 (JR274). While cruises JR247 and JR274 aimed to examine the pelagic shelf ecosystem by collection of predominantly water samples (and zooplankton during JR247) on the northern shelf, JC055 explored solely the composition of sediments on the South Georgia shelf. Cruise JR247 took place in January 2011 on RRS *James Clark Ross*, and 14 sites on the northern shelf and shelf edge of South Georgia were visited (stations

103   1 – 21; Fig. 1). Suspended particles were collected on acid cleaned polycarbonate filters (1

104   μm pore size; Whatman) using in-situ Stand-Alone Pumping Systems (SAPS; Challenger

105   Oceanic) attached to a Kevlar wire and deployed at 20 m, 50 m and 150 m depth (Fig. 1, red

106   dots). The filters were rinsed with deionized water (Milli-Q; Millipore), stored at -20°C, and

107   shipped frozen to the National Oceanography Centre Southampton (NOCS).

108   Subsurface seawater samples were collected by trace metal clean samplers (Ocean

109   Test Equipment (OTE)) at 9 of the 14 SAPS locations (Fig. 1; black stars). Seawater samples

110   were filtered using cartridge filter (0.2 μm Sartobran P300; Sartorius) into acid cleaned 125

111   mL low-density polyethylene (LDPE) bottles (Nalgene). Unfiltered samples were collected

112   in 125 mL LDPE bottles for analysis of total dissolvable (TD) trace metals. Surface waters

113   from the South Georgia shelf were collected using a tow fish deployed alongside the ship at 3

114   – 4 m depth. Samples were filtered in-line using a cartridge filter (0.2 μm Sartobran P300;

115   Sartorius) and dispensed in acid washed 125 mL LDPE bottles. Unfiltered surface seawater

116   samples were also collected and dispensed in acid washed 125 mL LDPE bottles. All

117   seawater samples were acidified on-board with ultra clean HNO_3 (15 M UpA grade, Romil)

118   to pH 1.7 (22 μmol H^+ L^{-1}). For a more detailed description of all sample-handling

119   procedures, please see Supplementary Text S1.

120   In January and February 2013, RRS *James Clark Ross* cruise JR274 revisited South

121   Georgia and collected surface seawater samples covering the shelf, shelf-edge, and open

122   ocean areas around the island. Dissolved and TD trace elements in surface seawater samples

123   were collected using the tow fish and treated similarly to samples from JR247. For a more

124   detailed description of all sample-handling procedures, please see Supplementary Text S1.

125   During the RRS *James Cook* cruise JC055 in February 2011, a megacorer (Bowers

126   and Connelly type) was used to collect surface sediment and pore water samples on the

127   southern side of South Georgia (there was no opportunity to sample the northern side of the

128 island). Cores representing the intact sediment – water interface were retrieved from three

129 sites on the southern shelf, at water depths of ca. 250 m (S1 – S3) (Fig. 1, blue hexagons).

130 Pore waters were separated by centrifugation under N_2 atmosphere and filtered using

131 cellulose nitrate syringe filters (0.2 μm pore size; Whatman (Homoky et al., 2012).

132 Conjugate sediments were freeze dried on board and stored at room temperature. A more

133 detailed description of sediment and pore water sample-handling procedures is provided in

134 Supplementary Text S2.

135 Krill faecal pellets were obtained during on-board krill incubations performed during

136 JR247. Incubations were performed in darkness in the laminar flow cabinet at ambient

137 surface layer temperature. The krill were incubated in filtered seawater from the tow fish for

138 up to ~3 h immediately after capture, so that pellets obtained derived from material ingested

139 in situ. These incubations and their results are described in more detail in Schmidt et al.

140 (2016).

141

142 **2.2 Trace metal analysis in suspended particles and krill faecal pellets**

143 The labile trace metal fraction of suspended particles (SAPS) and krill faecal pellets,

144 was remobilized using a 25% acetic acid solution (glacial SpA, Romil) following Planquette

145 et al. (2011). The labile trace metal fraction is hereafter referred to as the leachable trace

146 metal fraction (L). The remaining particles were digested on a hot plate applying a mixture

147 of aqua regia and hydrogen fluoride (Planquette et al., 2011). This fraction will be referred to

148 as the refractory fraction (R). The particulate trace metal fraction (P) is the sum of leachable

149 (L) and refractory (R). All samples were analysed by collision cell inductively coupled

150 plasma - mass spectrometry (ICP-MS) (ThermoFisher Scientific, XSeriesII). For more

151 detailed description of measured certified reference material see Supplementary Text S1.

152

2.3 Trace metal analysis of seawater

The filtered and unfiltered seawater samples were stored for a period of 12 months prior to analysis. Concentrations of dissolved and total dissolvable Fe, Mn, and Al in seawater were determined by off-line pre-concentration and isotope dilution / standard addition ICP-MS (ThermoFisher Scientific Element2 XR) according to Rapp et al. (2017). For a more detailed description of the method and measured reference materials see Supplementary Text S1.

2.4 Trace metal analysis of pore waters and sediments

Sub-samples of the bulk, homogenized sediments were fully dissolved following an aqua regia and combined hydrofluoric/perchloric acid digestion method following Homoky et al. (2011). The acid digests and pore waters were analysed by ICP-optical emission spectrometry (OES) (Perkin Elmer Optima 4300DV). For a more detailed description of the method and measured reference materials see Supplementary Text S2.

3. Results & Discussion

3.1 Supply routes of suspended particulate Fe, Mn, and Al

To avoid confusion, we will now define the terms biogenic, lithogenic, and authigenic particles, as they will be used frequently in the following sections. Biogenic particles refer to suspended organic particles, living and dead, such as phytoplankton cells. Lithogenic particles comprise mineral fragments, such as glacial flour and sediment particles. Authigenic particle include surface-scavenged trace metals and secondary minerals, such as amorphous $FeO(OH)$ (e.g. goethite), that are formed in seawater and because of their age are insoluble to weak acid leaches (e.g. 25% acetic acid solution).

3.1.1 Characterization of (the two) particulate trace metal fractions

178   Two different particulate fractions were obtained from samples collected during

179   JR247; a particulate fraction from suspended particles collected using 1 μm pore size SAPS

180   filters (P) and a leachable particulate fraction from unfiltered acidified seawater samples

181   (LP_{Un}) collected at the same depth. LP_{Un} was calculated following Eq. (1):

182   LP_{Un} = total dissolvable (TD; unfiltered) – dissolved (D; 0.2 μm filtered)   (1)

183   Because of the different sampling approaches (SAPS vs. OTE water samplers), filter sizes

184   (>1 μm for SAPS vs. >0.2 μm for dissolved seawater) and digestion procedures (aqua regia +

185   HF for SAPS particles vs. water sample storage at pH 1.7 [22 μmol H^+ L^{-1}]), concentrations

186   of LP_{Un} and P differed, but showed similar distribution patterns in the water column (Fig. 2

187   and S1, Table 1 and 2). The concentrations of Fe, Mn and Al in the LP_{Un} fraction ($LP_{Un}Fe$,

188    $LP_{Un}Mn$, $LP_{Un}Al$) were usually slightly lower than the particulate fraction from suspended

189   particles (PFe, PMn, PAl). The LP_{Un} of unfiltered seawater samples corresponded to ~ 63 ± 4

190   % of the PFe, 83 ± 11% of the PAl and nearly 100 ± 10% of the PMn fractions obtained by

191   SAPS. The average LP_{Un} trace metal ratios ($LP_{Un}Fe$/ $LP_{Un}Mn$ = 33.07 ± 3.45 (1 σ) and

192    $LP_{Un}Fe$/ $LP_{Un}Al$ = 0.65 ± 0.10 (n=69)), were about half of the elemental ratios of suspended

193   particles obtained by SAPS (PFe/PMn = 68.0 ± 0.6 and PFe/PAl = 1.251 ± 0.042 (n=42) (Fig.

194   3; Table 1, 2 and 3)).

195   The lower concentrations of Fe and Al and the reduced elemental ratios in the LP_{Un}

196   compared to the P fractions suggests that an unknown fraction of particulate Fe and Al in

197   seawater was not leached during the acidification procedure at pH 1.7 over 12 months.

198   However, since P and LP_{Un} displayed similar trends with depth (Fig. 2 and S1), LP_{Un} was

199   used in sections 3.1.3 and 3.3 as an indicator for the abundance of particulate trace metals at

200   locations where particulate samples could not be retrieved by SAPS, e.g. in surface waters

201   collected by the tow fish and depths greater than 150 m.

202

203 3.1.2 Suspended particulate trace metals in the water column

204   Concentrations of PFe, PMn and PAl in the water column ranged from $0.87 - 267$

205 nmol L^{-1}, $0.01 - 3.85$ nmol L^{-1}, and $0.60 - 195$ nmol L^{-1}, respectively (Fig. 2, Table 2).

206 Concentrations of $LP_{Un}Fe$, $LP_{Un}Mn$ and $LP_{Un}Al$ ranged from $1 - 118$ nmol L^{-1}, $0.01 - 100$

207 nmol L^{-1}, and $1 - 141$ nmol L^{-1}, respectively (Fig. 2, Table 1). Below the isopycnal density

208 layer 27.05 kg m^{-3}, located at $\sim 50 - 70$ m depth, P and LP_{Un} increased with depth and showed

209 a maximum near the seafloor of e.g. 207 nmol L^{-1} for PFe and 112 nmol L^{-1} for $LP_{Un}Fe$ (#17,

210 Table 2). Most sites on the shelf (bottom depth $\leq$ 260 m; #9/10, #13, #14, #17, and #21)

211 showed seafloor maxima, in agreement with other shelf studies. For example, Milne et al.

212 (2017) reported concentrations of up to 140 nmol L^{-1} for PFe and 800 nmol L^{-1} for PAl in

213 bottom waters on the west African shelf, and Chase et al. (2005) showed bottom water

214 maxima of up to 400 nmol L^{-1} for $LP_{Un}Fe$ off the Oregon coast.

215   Strong linear relationships between elements were observed for suspended particles

216 (SAPS) obtained from above and below the 27.05 kg m^{-3} isopycnal, with elemental ratios of

217 PFe/PMn = 68.0 ± 0.6, PFe/PAl = 1.25 ± 0.04 and PMn/PAl = 0.0171 ± 0.0041 (n=42) (Fig.

218 3, Table 2 and 3). These elemental ratios were higher than those reported for the earth's crust

219 (Fe/Mn = 58.0, Fe/Al = 0.2, Mn/Al = 0.0035 (Wedepohl, 1995)) and sediment samples

220 collected to the south of the island (mean sediment surface layer of S1, S2, S3; SFe/SMn =

221 51.5 ± 2.4, SFe/SAl = 0.34 ± 0.02, SMn/SAl = 0.0066 ± 0.0002 (Fig. 4, Table 3 and 4)),

222 suggesting that the suspended particles were more enriched in Fe than crustal and lithogenic

223 particles (Table 3).

224   The Fe/Mn ratios among different phytoplankton species show strong variations but

225 are typically much lower (Fe/Mn $\sim$ 1.7 (Ho et al., 2003)), with also lower Fe concentrations

226 than lithogenic (sediment) particles (cellular Fe concentration of phytoplankton $\sim$ 0.7 mmol

227 kg^{-1} (Ho et al., 2003); upper crust $\sim$ 550 mmol kg^{-1} (Wedepohl, 1995)). A prevalence of

228 biogenic particles in the suspended particle pool would be expected to result in reduced

229 PFe/PMn ratios in our SAPS samples to values less than 51.5 as was observed in the

230 sediments.

231 It is most likely that authigenic Fe precipitation (e.g. DFe was scavenged onto

232 sediment particles) increased the Fe to Al (and Fe to Mn) ratio of suspended particles

233 (PFe/PAl = 1.25; PFe/PMn = 68.0) compared to sediment particles (SFe/SAl = 0.34;

234 SFe/SMn = 51.5). At seawater pH (~pH 8), dissolved Fe(III) is rapidly hydrolysed to soluble

235 Fe(III)(OH)$_3$ (< 0.02 µm) which readily accumulates as nanometer sized colloids (0.02 – 0.2

236 µm) (Liu and Millero, 2002) and particles (> 0.2 µm) (own observation). It has been also

237 shown that both soluble and colloidal Fe are attracted by charged surfaces (organic and

238 inorganic particle surfaces), a process that removes DFe and simultaneously increases the

239 amount of particulate Fe in seawater over time (Schlosser et al., 2011).

240 A range of mechanisms delivers suspended particles to the surface waters. These

241 transport mechanisms will be discussed in the following section.

242

243 3.1.3 Glacial outflow and zooplankton feeding activity

244 While most stations on the shelf showed bottom water maxima of particulate metals,

245 at three sampling sites located on the shelf (#18) and shelf edge (#15/16 and #19/20), the

246 particulate trace metal concentrations featured maxima in the top 100 m of the water column

247 (Fig. 2 and 5). At site #19/20, ca. 100 km away from the coast with a water depth of 1,741 m,

248 the PFe concentration at 20 m depth was 97 nmol L^{-1}, similar to LP$_{Un}$Fe (Fig. 5). The

249 elemental ratio PFe/PAl of these samples (e.g. 1.01 for site #19/20, 20 m depth) were close to

250 the average ratio (PFe/PAl = 1.25), indicating that lithogenic and authigenic Fe dominated the

251 suspended particulate pool in these surface waters.

252   The surface water maxima of trace metals could have two supply routes: 1) lateral

253 transport of waters containing lithogenic and authigenic particles from shallow island shelf

254 sediments, and 2) transport of glacial particles following melt processes. The reduced

255 salinities (~33.3 PSU) recorded in surface waters in Cumberland Bay and ~50 km offshore of

256 South Georgia (~33.8) (Fig. 6(c) and S2) provide an indication of glacial outflow, melting of

257 icebergs and run-off of melt water streams. Enhanced $LP_{Un}Fe$ concentrations of 2.2 μmol L^{-1}

258 in low salinity surface waters inside Cumberland Bay, are indicative of a meltwater source

259 (LP_{Un} concentration used as only water samples from the tow fish available). The $LP_{Un}Fe$

260 concentration decreased strongly with increasing distance from the coast, and exhibited an

261 abrupt reduction to $1 - 5$ nmol Fe L^{-1} at the shelf edge ~ 100 km offshore. A similar

262 distribution pattern was observed for $LP_{Un}Mn$ (Fig. 6(d)) and $LP_{Un}Al$ (not shown), for cruises

263 JR247 and JR274. Glacial melt has been reported as an important source of particulate

264 material in the vicinity of the Antarctic Peninsula (de Jong et al., 2012). For example,

265 Gerringa et al. (2012) documented elevated total dissolvable Fe concentration of up to 106

266 nmol L^{-1} near the Pine Island Glacier in the Amundsen Sea, and Raiswell et al. (2008)

267 estimated that per year 1.6 Gmol nanoparticulate Fe, associated to lithogenic particles, are

268 delivered to the Southern Ocean by melting ice.

269   Locally elevated particulate metal concentrations in surface waters may also be

270 related to production of faecal pellets by swarms of Antarctic krill (Schmidt et al., 2016).

271 High abundances of Antarctic krill were estimated from acoustic backscattering observations

272 (Fielding et al., 2014), and large numbers of faecal pellets were observed on the SAPS filters

273 during cruise JR247. The stomach content of Antarctic krill contained up to 90% sediment

274 particles by volume, an observation that was attributed to filter feeding by these organisms on

275 phytoplankton and seabed detritus, with incidental ingestion of deep ocean sediments

276 (Schmidt et al., 2011) and glacial flour (Schmidt et al., 2016). Krill thus take up lithogenic

277 (sediment) particles and transfer these into the surface ocean through the egestion of faecal

278 pellets (Schmidt et al., 2016). The trace metal contents of krill faecal pellets collected during

279 on-board incubation experiments during JR247 ranged from 0.88 – 67.14 µg Fe mg^{-1} dry

280 weight (n = 27) (Table 5) (Schmidt et al. 2016). The molar ratio PFe/PAl = 0.48 ± 0.07 and

281 PMn/PAl = 0.0069 ± 0.001 of the faecal pellets was similar to those for sediment particles

282 (SFe/SAl = 0.34 ± 0.02 and SMn/SAl = 0.0066 ± 0.001; Table 1, 2, 3 and 4), indicating that

283 Fe in krill faecal pellets was predominately associated with lithogenic (sediments) and/or

284 glacial flour particles, as also reported by Schmidt et al. (2016). In contrast, the molar ratio

285 PFe/PMn = 70.65 ± 8.22 of faecal pellets was higher than that of sediments, SFe/SMn = 51.5

286 ± 2.4, but just slightly higher than that of suspended SAPS particles, PFe/PAl = 68.0 ± 0.6.

287 The observed variability in the PFe/PAl and PFe/PMn ratio in the various particle pools is

288 therefore a consequence of different amounts of lithogenic and authigenic particles.

289

290 **3.2 Supply routes of dissolved Fe, Mn, and Al**

291   Concentrations of DFe, DMn, and DAl in the water column showed strong variations

292 and ranged from ~ 0.1 – 25.9 nmol L^{-1}, 0.3 – 19.6 nmol L^{-1} and 0.1 – 18.4 nmol L^{-1},

293 respectively (Fig. 2, 5 and 7), with highest values in the surface waters in Cumberland Bay,

294 and lowest beyond the shelf break (Fig. 6). Dissolved Fe concentrations from this study are

295 in agreement with reported DFe near the Antarctic Peninsula (0.6 – 14.6 nmol L^{-1} (de Jong et

296 al., 2012)) and Crozet Islands (0.1 – 2.5 nmol L^{-1} (Planquette et al., 2007)). Sources and

297 sinks of dissolved trace metals, and their distribution in the water column are discussed in the

298 following sections.

299

300 3.2.1 Supply from sediment pore waters

301   Elevated pore water concentrations of Fe and Mn (Fe_{PW} and Mn_{PW}) were observed in

302   sediments from the southern shelf sites at water depths of around 250 m, and ranged from 0.5

303   – 110 µmol L^{-1} for Fe and 0.1 – 2 µmol L^{-1} for Mn (Fig. 7 and Table S2). The down-core

304   distributions of Fe_{PW} and Mn_{PW} were consistent with microbial dissimilatory Mn and Fe

305   reduction during organic matter oxidation (Canfield and Thamdrup, 2009), and thus

306   concentrations were elevated at defined depth horizons controlled by their redox potential

307   (Eh) (Bonneville et al., 2009; Raiswell and Canfield, 2012).   The Fe_{PW} and Mn_{PW}

308   concentrations near the sediment-seawater interface were used to calculate fluxes of Fe and

309   Mn to bottom waters following diffusion of reduced Fe and Mn species across an oxygenated

310   layer in surface sediments. These calculations were performed following Boudreau and Scott

311   (1978) and Homoky et al. (2012), and are described in detailed in the Supplementary Text S3

312   and Table S1. We are aware that our calculated fluxes represent minimum estimates of pore

313   water efflux, which under natural conditions is supplemented by advection due to

314   bioirrigation, bioturbation, and bottom water currents (Homoky et al., 2016). In addition,

315   sediment cores were collected on the southern shelf, while seawater and particulate samples

316   were collected on the northern shelf side. The benthic Fe fluxes for the southern shelf maybe

317   lower than those on the northern shelf, as an elevated primary productivity and enhanced

318   particle export on the northern side will result in enhanced bacterial respiration, which

319   reduces Eh and promotes the dissolution of Fe oxides with subsequent release of Fe into

320   bottom waters.

321   Notwithstanding the above issues, we calculated substantial benthic fluxes from

322   sediment pore waters to bottom waters on the southern shelf for Fe_{PW} of <0.1 to 44.4 µmol m^{-2} d^{-1}

323   and Mn_{PW} of 0.6 to 4.1 µmol m^{-2} d^{-1}. The upper flux values for Fe are comparable to

324   those reported for dysoxic and river-dominated continental margins (3.5 – 55 µmol m^{-2} d^{-1}

325   (Homoky et al., 2012)), seasonal maxima of temperate and oxic shelf seas (23 – 31 µmol m^{-2}

14

326 d^{-1} (Klar et al., 2017)), and shelf sediments off the Antarctic Peninsula (1.3 – 15.5 μmol m^{-2}

327 d^{-1} (de Jong et al., 2012)). The Mn fluxes were relatively low for shelf environments, with for

328 example fluxes of 70 – 4450 μmol m^{-2} d^{-1} reported for Baltic and Black Sea sediments

329 (Pakhomova et al., 2007)). The Fe pore water fluxes from the South Georgia shelf sediments,

330 which extend over an area of ca. 40,000 km^2, indicate that these may serve as an important

331 year-round source to overlying waters, totalling 4 to 1,728 kmol DFe d^{-1} and 25 to 164 kmol

332 DMn d^{-1}.

333   Benthic release of trace metal enriched pore waters shaped the distributions of

334 dissolved trace metals in bottom waters on the shelf. Concentrations of DFe, DMn, and DAl

335 were enhanced at isopycnals > 27.05 kg m^{-3} (e.g. DFe up to 7.70 nmol L^{-1} at site #21, Table

336 1) compared to surface waters (e.g. DFe as low as 0.30 nmol L^{-1} at site #13, Table 1; Fig. 2

337 and 7). Trace metal enriched bottom waters were also observed at sites #13, #14, #17 and

338 #18 (Fig. 2). The molar DFe/DMn ratios in oxygenated bottom waters varied between 1.1 –

339 3.5 and were thus similar to pore waters near the sediment-seawater interface (0 – 1 cm

340 depth, Fe$_{PW}$/Mn$_{PW}$ = 2.2 ± 1.0; Fig. 7). The similar trace metal ratios suggest that Fe and Mn

341 in enriched pore waters crossed the sediment-bottom water interface and accumulated in shelf

342 bottom waters.

343   To determine the vertical DFe fluxes from near bottom to surface waters we

344 employed a method outlined by de Jong et al. (2012), and calculated both the advective and

345 diffusive flux terms, which are not affected by the benthic Fe and Mn fluxes. We included

346 the advective term in our calculations, because it has been shown that internal waves that

347 cross shallow topographies and wind shear stress produces strong turbulence that facilitate

348 Eckman upwelling (vertical advection) on the shelf (Kurapov et al., 2010; Moore, 2000;

349 Wolanski and Delesalle, 1995). Applying literature values from the Southern Ocean for

350 vertical diffusivity (K_Z = 1 x 10^{-4} m^2 s^{-1} (Charette et al., 2007)) and advective velocity (w =

351   1.1×10^{-6} m s^{-1} (de Jong et al., 2012)), an average vertical DFe flux on the shelf of 0.41 ±

352   0.26 µmol m^{-2} d^{-1} from subsurface waters into the surface mixed layer was estimated

353   (Supplementary Text S4). The surface mixed layer depth was determined by a density

354   criteria (~0.03 kg m^{-3} (de Boyer Montégut et al., 2004)) and was located at ~50 m depth.

355   About 38% of the DFe flux was related to Ekman upwelling (advective term) and 62% to the

356   diffusive flux. This vertical flux is at the lower end of the calculated benthic flux from this

357   study (Fe$_{PW}$ < 0.1 to 44.4 µmol m^{-2} d^{-1}), and agrees with values reported for other Southern

358   Ocean shelf regions near the Antarctic Peninsula (within 20 – 70 km from the coast: ~ 2.7 ±

359   3.4 µmol m^{-2} d^{-1} (de Jong et al., 2012)) and the Crozet Islands (only diffusive flux of 0.06

360   µmol m^{-2} d^{-1} (Planquette et al., 2007)).

361

362   3.2.2 DFe supply from the leachable fraction of particles

363   The analytical protocol for the analysis of SAPS-collected particulate material allows

364   separate estimation of the refractory and leachable fractions of trace elements (R and L,

365   respectively). The R fraction of the suspended matter is considered to include silicates and

366   aged oxide minerals, while the L fraction represents predominantly fresh oxyhydroxides,

367   biogenic material and loosely bound surface associated elements which are readily

368   remobilized using leaching procedures (Berger et al., 2008).

369   Concentrations of LFe, LMn and LAl in the water column showed strong variations,

370   ranging from a few picomoles to several nanomoles L^{-1} (Table 2). On average, LFe and LAl

371   concentrations at 150 m depth (~ 1.3 nmol LFe L^{-1} and ~0.95 nmol LAl L^{-1}) were

372   significantly higher than at 20 and 50 m, LFe = 0.3 nmol L^{-1} (student t-test: t[0.95;28] =

373   1.725 [1.703]; t[confidence level; n-1]); LAl = 0.43 nmol L^{-1} (student t-test: t[0.90;28] =

374   1.383 [1.313]). The LMn concentrations did not vary strongly and remained near constant

375   throughout the top 150 m (LMn = 8.9 pmol L^{-1} {student t-test: [0.65;28] = 0.400 [0.390]}).

The average contribution of L to the particulate pool P (R+L), was low; 0.83 ± 1.13% for Fe, 2.55 ± 1.58% for Mn and 2.42 ± 1.32% for Al (Table 2). A study conducted in the North Pacific near the Columbia River outflow, reported considerably higher L fractions (e.g. 6.6±3.0% of Fe, 78.7±14.0% of Mn, 6.3±2.0% of Al (Berger et al., 2008)), which was attributed to enhanced biogenic particle levels in the low salinity waters of the river (Berger et al., 2008). In contrast, results from our study showed that particulate trace metals predominately had a refractory component (R), indicating that Fe, Mn, and Al was mainly incorporated in mineral structures unaffected by a weak acid leach (e.g. aged oxyhydroxides and alumosilicates).

A weak linear relationship between R and L was observed for Fe ($R^2 = 0.57$, n = 41), Mn ($R^2 = 0.64$, n = 41) and Al ($R^2 = 0.63$, n = 41) (Supplementary Fig. S3 and S4), indicating that the L fraction included mainly lithogenic and authigenic (e.g. scavenged) Fe, Mn and Al and not much LFe was incorporated in biogenic particles. The scavenging of dissolved trace metals by charged particle surfaces is established (Homoky et al., 2012; Koschinsky et al., 2003), but how well Fe and other trace metals can be remobilized from marine particle surfaces and which process may modify their availability over time is not yet well constrained (Achterberg et al., 2018; Fitzsimmons and Boyle, 2014; Milne et al., 2017).

For instance, scavenged Fe is reported to exchange with DFe in the water column of the tropical and high latitude North Atlantic (Achterberg et al., 2018; Fitzsimmons and Boyle, 2014; Milne et al., 2017). In addition, recent work has concluded that zooplankton grazing and the production of faecal pellets remobilizes DFe from lithogenic and biogenic particles (Giering et al., 2012; Schmidt et al., 2016). In contrast, freshly produced inorganic Fe(III) oxyhydroxide (FeOOH * nH_2O) precipitates in seawater are accessible but are subject to chemical and structural conversions that lead to less leachable Fe with time (Yoshida et al., 2006).

401

402   3.2.3 DFe supply from Antarctic krill

403   Elevated dissolved trace metal concentrations in the top 200 m of the water column

404   coincided with elevated particulate trace metal concentrations at sites #11/12, #15/16, #18,

405   and #19/20 (Fig. 2, 5, and 7). The SAPS filters from these stations contained a high load of

406   krill faecal pellets. To elucidate the relationship between dissolved trace metal

407   concentrations and the local abundance of Antarctic krill and their faecal pellets, krill were

408   caught and incubated on-board the vessel as described in Schmidt et al. (2016).

409   Antarctic krill excretion rates of DFe were variable, relating positively to the extent

410   of recent ingestion of diatoms. However, on average krill released ~2.0 ± 1.9 nmol DFe

411   individual^{-1} d^{-1} (Schmidt et al., 2016). By applying a mean krill abundance of 465 ± 588

412   individuals m^{-2}, estimated from acoustic backscattering measurements (Fielding et al., 2014),

413   krill excreted 1.1 ± 2.2 μmol DFe m^{-2} d^{-1} into the top 300 m of the water column (Schmidt et

414   al., 2016). In addition, krill produced ca. 1.8 ± 1.6 mg of faecal pellets per individual per day,

415   containing ca. 0.30 ± 0.33 μmol Fe mg^{-1}. Particle leaches performed on those faecal pellet

416   samples with 25% acetic acid showed that on average 2.5 ± 2.1% (9.3 ± 13.3 nmol Fe mg^{-1})

417   of the total Fe in these pellets could be remobilised (Table 5), which would equate to a

418   production of 14 ± 24 nmol LFe ind^{-1} d^{-1}. By multiplying the mean LFe by the ambient krill

419   density used above, we calculate a LFe flux of 6.5 ± 8.2 μmol m^{-2} d^{-1} from the faecal pellets

420   to the water column.

421   Since krill are mobile animals, questions remain over where the major part of the LFe

422   flux occurs, and what the fate of this Fe source is. Highest krill abundances were recorded

423   generally (but not exclusively) in the top 100 m layer (Fielding et al., 2014), and hence a

424   large proportion of this LFe flux from krill is likely to occur in the upper waters.

425   Notwithstanding our current uncertainties over the depths of origin and fate, the LFe flux

18

426 from krill faecal pellets and the release of DFe were on average an order of magnitude higher

427 than estimated vertical diffusive and advective DFe fluxes, with other grazers, such as

428 copepods and salps, adding to the recycled flux estimates. This illustrates the importance of

429 zooplankton-mediated-Fe-cycling, in agreement with previous studies (Hutchins and Bruland,

430 1994; Sato et al., 2007).

431   The experimental set-up did not allow us to establish the origin of the Fe released by

432 krill, being both "recycled" Fe from biogenic material and "new" Fe from lithogenic (and

433 authigenic) material. However, Schmidt et al. (2016) concluded that zooplankton gut passage

434 mobilizes lithogenic Fe, and showed that there are strong spatial patterns in the organic and

435 lithogenic make-up of faecal pellets. This included an exponential decline in the quantity of

436 lithogenic particles in krill stomachs with distance from sources of glacial flour on the

437 northern South Georgia coast. For instance, the lithogenic content at one site on the shelf

438 contributed ~90% of stomach content volume suggesting that a large quantity of the

439 accessible Fe was remobilized from those inorganic particles.

440

441 **3.3 Off-shore transport of trace metal enriched water masses**

442   Along a W – E transect (Fig. 1; #14 via # 13 to #11/12), lateral water mass transport

443 carried suspended particles offshore. Because of the small size of the SAPS particulate data

444 set (two data points), we considered the LP_{Un} fraction for this transect (Fig. 1). Indeed,

445 elevated concentrations of the P and LP_{Un} metal fractions were observed in subsurface waters

446 that had been in recent contact with the shelf. These metal-enriched waters, detected at the

447 eastern shelf edge site #11/12 between 200 and 400 m water depth (Fig. 1 and 4), exhibited

448 similar temperature and salinity signatures to shelf bottom waters. Furthermore, the

449 elemental ratios of the LP_{Un} fraction in these waters were similar to the particles in the surface

450 sediments (S1, S2, and S3) and the resuspended particles in the bottom boundary layer (#13

451   and #14) on the shallow shelf (Fig. 4). A similar distribution was also found for the P

452   fractions, but limited to site #13 and #14, as SAPS were not deployed below 150 m at the

453   shelf edge site #11/12.

454   The $LP_{Un}Fe$ concentration decreased with distance from the island to offshore: from

455   site #14 at 200 m depth ($LP_{Un}Fe = 82.26$ nmol L^{-1}; water depth = 255 m) to site #13 at 100 m

456   depth ($LP_{Un}Fe = 34.06$ nmol L^{-1}; water depth = 130 m) to site #11/12 between 200 and 400 m

457   depth ($LP_{Un}Fe \sim 10.18$ nmol L^{-1}; water depth = 750 m) (Fig.4 and Table 1). A similar

458   decrease was observed for the SAPS Fe data: from site #14 at 150 m depth (PFe = 31.12

459   nmol L^{-1}) to site #13 at 100 m depth (PFe = 10.23 nmol L^{-1}). The decrease of PFe and

460    $LP_{Un}Fe$ with increasing distance to the coast is in agreement with previous observations for

461   the Western Subarctic Pacific (Lam and Bishop, 2008), which reported elevated LFe

462   concentrations in the range of 0.6 to 3.8 nmol L^{-1} in subsurface waters between 100 and 200

463   m depth along the Kamchatka shelf and related this observation to offshore water mass

464   transport. However, we assume that particles in the deep particulate Fe maximum are not

465   transported over very large distances, due to their tendency to sink, and thus do not

466   significantly contribute to the offshore Fe supply (section 3.4).

467   Consistent with the observed P and LP_{Un} distributions, elevated dissolved metal

468   concentrations at depths between 200 and 400 m at site #11/12 indicated that trace metal

469   enriched shelf bottom waters were transported offshore (Fig. 7). However, dissolved trace

470   metal concentrations were more variable than P and LP_{Un}, and in case for DMn were highest

471   at depths at shelf edge site #11/12. Notwithstanding the above issue, for horizontal flux

472   calculations we used the entire DFe data set for water depths between 100 and 400 m.

473   Average DFe concentrations in this depth range were highly variable and did not follow an

474   exponential or power law function with distance from the coast (Supplementary Fig. S5),

475 which is necessary to determine scale length and horizontal diffusivity (K_h) (de Jong et al.,

476 2012). As a result, horizontal flux calculations from the data could not be executed.

477 The distribution of dissolved trace metals in surface waters indicated that there was a

478 limited transfer of DFe beyond the shelf break into the bloom region. Surface samples

479 showed that DFe concentrations were strongly enriched in surface waters on the shelf (0.3 –

480 25.9 nmol L^{-1}, Fig. 6(b)), while DFe concentrations beyond the shelf break decreased

481 abruptly to concentrations < 0.2 nmol L^{-1} (Fig. 6(b)). This indicates that DFe was quickly

482 removed from ACC surface waters following passage of the island. However, previous

483 studies in the region suggest DFe transfer beyond the shelf break of South Georgia (Borrione

484 et al., 2013; Nielsdóttir et al., 2012). Nielsdóttir et al. (2012) reported surface waters

485 downstream the island shelf with up to 2 nmol DFe L^{-1}, with seasonal variations and highest

486 concentrations during austral summer in January/February 2008. Dissolved Fe data from

487 JR247 (2011) and JR274 (2012) were also obtained during the summer season, but indicated

488 rapid reduction in concentrations through mixing with DFe depleted ACC water, biological

489 uptake and/or particle scavenging (authigenic precipitation).

490

491 **3.4 Iron budget in the bloom region**

492 Large seasonal phytoplankton blooms downstream of South Georgia recorded by

493 earth observing satellites are initiated by Fe supplied by the South Georgia island/shelf

494 system during the passage of ACC waters (Fig. 1) (Borrione et al., 2013; Nielsdóttir et al.,

495 2012). Based on our study, the main DFe sources during this passage of the ACC were

496 benthic release and vertical mixing, release of DFe from krill and krill faecal pellets, and

497 supply of particles from run-off and glacial meltwater. In the following sections we will

498 discuss the strength of each DFe source in the bloom region ca. 1,250 km downstream of the

499 island and estimate how much DFe is required to stimulate the elevated primary productivity

500   in that region. Because of the lack of observational data for the region, this part of the study

501   combines literature values from different Southern Ocean studies. This approach contains

502   large uncertainties that are discussed in detail in Section 3.4.6 Budget uncertainties.

503

504   3.4.1 Phytoplankton Fe requirements in the phytoplankton bloom region

505   The surface ocean in the vicinity of South Georgia during the austral summer features

506   strongly elevated biomass production (Gilpin et al., 2002) and represents the largest known

507   CO_2 sink in the ACC (12.9 mmol C m^{-2} d^{-1} (Jones et al., 2012)). The Fe requirements of the

508   phytoplankton community in austral summer within the bloom that reaches several hundred

509   kilometres downstream the island were determined by combining satellite-depth integrated

510   net primary production data derived from a phytoplankton pigment adsorption (α_{ph})-based

511   model (62 ± 21 mmol C m^{-2} d^{-1} (Ma et al., 2014)) over the period of 2003-2010 with an

512   average intracellular Fe/C ratio obtained from five Southern Ocean diatom species (5.23 ±

513   2.84 µmol Fe mol^{-1} C (Strzepek et al., 2011)). This approach yielded an approximate Fe

514   requirement of 0.33 ± 0.11 µmol DFe m^{-2} d^{-1} for the phytoplankton community (Fig. 8). For

515   a more detailed description of the applied values and calculations see Supplementary Text S4.

516

517   3.4.2 Horizontal and vertical mixing

518   De Jong et al. (2012) reported that horizontal and vertical advective, diffusive

519   (diapycnal) and deep winter mixing downstream (1,250 – 1,570 km) of the Antarctic

520   Peninsula (between 51°S and 59°S) supplied DFe to the surface waters in quantities that

521   exceeded the DFe requirement of primary producers during austral summer (0.13 ± 0.04

522   µmol DFe m^{-2} d^{-1}). In their study region, de Jong et al. (2012) determined that ~ 0.30 ± 0.22

523   µmol DFe m^{-2} d^{-1} were supplied by horizontal and vertical fluxes, of which 91% of the

524   vertical flux were attributed to Ekman upwelling (advective term), and 43% of the entire DFe

525 flux was supplied by deep winter mixing. Tagliabue et al. (2014) reported similar model

526 estimates for the region that is located south of the Polar Front and characterized by strong

527 Ekman upwelling and winter entrainment.

528   For the bloom region downstream of South Georgia, model calculations by Tagliabue

529 et al. (2014) indicated that less than 0.0003 μmol DFe m^{-2} d^{-1} were supplied by diapycnal

530 mixing, and ~ -0.0027 μmol DFe m^{-2} d^{-1} were removed by Ekman down-welling. For the

531 vertical flux component, this yields an overall loss of DFe of ~ -0.002 μmol DFe m^{-2} d^{-1}

532 (0.0003 + (-0.0027)) in the bloom region north of South Georgia (Fig. 8).

533   Because the sampling in our study was not suitable for calculations of the horizontal

534 flux, we applied the horizontal flux estimates from de Jong et al. (2012) for our own Fe

535 budget. For a region ca. 1,250 km downstream of a source, calculations according to de Jong

536 et al. (2012) sugest that ca. 0.11 ± 0.03 μmol DFe m^{-2} d^{-1} are supplied to the bloom region by

537 horizontal advection and diffusion (Fig. 8).

538

539 3.4.3 Deep winter mixing

540   The entrainment of new DFe during winter represents an important Fe source to

541 surface waters in the Southern Ocean (de Jong et al., 2012; Tagliabue et al., 2014). Elevated

542 DFe concentrations in subsurface waters support primary production in the austral spring

543 following entrainment by deep winter mixing. Model estimates showed that DFe supplied by

544 winter mixing, together with diapycnal mixing, matches the Fe requirements at most low

545 productivity sites in the Southern Ocean. However, deep winter mixing at the highly

546 productive sites north of South Georgia supplies only ~ 0.011 μmol m^{-2} d^{-1} (Tagliabue et al.,

547 2014) (Fig. 8). Later in the season primary productivity in surface waters is considered to rely

548 strongly on Fe derived from recycling of biogenic material (Boyd et al., 2015).

549

550   3.4.4 Dust deposition

551   Dissolved Fe supplied by the deposition of aeolian dust is considered to be an

552   important source to the Southern Ocean (Conway et al., 2015; Gabric et al., 2010; Gassó and

553   Stein, 2007). Aeolian flux model estimates, supplied by Borrione et al. (2013) using a

554   regional South Georgia model, suggested that up to 8 µmol Fe m^{-2} d^{-1} are delivered to the

555   bloom regions downstream of South Georgia by dry and wet deposition. However, reliable

556   dry and wet deposition estimates for the Southern Ocean are limited. Data from the South

557   Atlantic along 40°S, ~ 1.000 km north of South Georgia, showed that rather low levels of

558   DFe (~ 0.002 µmol m^{-2} d^{-1}) are supplied by dry deposition (Chance et al., 2015). In addition,

559   ~ 1.0 ± 1.2 µmol DFe m^{-2} d^{-1} are delivered sporadically to the 40°S area by wet deposition

560   (Chance et al., 2015). However, even when assuming that similar wet deposition fluxes

561   occur north of South Georgia, fertilization with DFe is temporally and spatially limited.

562   Furthermore, it is very unlikely that such sporadic events could cause long-lasting and far

563   extending phytoplankton blooms strictly constrained between the PF and the SACCF.

564

565   3.4.5 Luxury Fe uptake on the shelf

566   Our conservative estimate of DFe supply to the bloom region by vertical/horizontal

567   mixing, deep winter entrainment and dust deposition (< 0.12 µmol Fe m^{-2} d^{-1}) covers only

568   ~30% of the estimated phytoplankton requirements (~ 0.33 µmol Fe m^{-2} d^{-1}) (Fig. 8). We

569   hypothesize that the missing supply of ~ 0.21 µmol DFe m^{-2} d^{-1} is supplied to the bloom

570   region through the off-shore advection of phytoplankton cells that are enriched in labile Fe.

571   It has been demonstrated that Fe-rich biogenic particles can be created by luxury iron uptake

572   of diatoms (Iwade et al., 2006; Marchetti et al., 2009). Using bottle incubation experiments,

573   Iwade et al. (2006) showed that under Fe replete conditions the coastal diatom *Chaetoceros*

574   *sociale* stores more intracellular Fe than needed for the production of essential enzymes and

575 proteins. We therefore hypothesize that phytoplankton cells that grew under excess nutrient

576 supply on the South Georgia shelf stored more Fe than needed for their metabolic processes.

577 Due to subsequent cycles of grazing, lysis or bacterial decomposition, this iron can be

578 remobilised in surface waters and made available for renewed phytoplankton uptake.

579 High Fe recycling efficiencies, described by the fe ratio (Boyd et al., 2005), are

580 required to maintain the cycle of remineralisation and uptake in the euphotic zone. This

581 counteracts the loss of particulate Fe by vertical export. Boyd et al. (2015) reported the

582 highest recycling efficiencies of ~ 90% for subantarctic, DFe-deplete waters such as

583 downstream of South Georgia. Further, these workers showed that the degree of recycling is

584 controlled by the abundance of prokaryotes with a high Fe quota, such as cyanobacteria, and

585 particularly by grazing zooplankton. The waters off South Georgia feature among the highest

586 biomasses worldwide of metazoan grazers (Atkinson et al., 2001). These large grazers,

587 chiefly copepods and Antarctic krill, are able to efficiently ingest large diatoms including

588 species that are known to store luxury iron (Atkinson, 1994; Hamm et al., 2003), thereby

589 disintegrating cell membranes and releasing trace metals.

590 In recent years it has become apparent that the recycling of biogenic particles in the

591 euphotic zone is a critical mechanism that maintains primary production, especially when the

592 dissolved nutrient pools become exhausted (Boyd et al., 2015; Tagliabue et al., 2014).

593 However, uncertainties remain over the degree to which Fe is lost during each cycle of uptake

594 and remineralisation. Thus more research is needed, especially field work that encompasses

595 the community structures (bacteria, phytoplankton, zooplankton, and higher predators

596 (Ratnarajah et al., 2017; Wing et al., 2014)), the degree of recycling for macro- and micro-

597 nutrients in the euphotic zone, and loss of Fe through vertical export.

598 An alternative explanation to our suggestion that recycling of luxury iron enriched

599 biota contributes to the downstream bloom is that iron is adsorbed directly onto particles that

600 are advected directly offshore. For example freshly precipitated Fe(III) oxyhydroxides

601 (FeOOH * nH$_2$O) may be adsorbed onto biogenic and non-biogenic material. Iron freshly

602 absorbed onto biogenic and non-biogenic material can be released and incorporated by

603 phytoplankton and bacteria. However, the bioavailability of adsorbed and inorganic Fe

604 changes over time. Both Wells et al. (1991) and Chen and Wang (2001) demonstrated that

605 the bioavailability of freshly precipitated FeOOH and Fe adsorbed onto colloids/inorganic

606 particles decreases over time. This is primarily due to the dehydration of the loosely packed

607 structure that is subsequently transferred into amorphous FeOOH in the mineral structure

608 Goethite. Because of this we suggest that the majority of Fe from inorganic FeOOH or Fe

609 adsorbed onto particles must be released and utilized in an early stage of the voyage, mainly

610 on the shelf or shortly after the shelf break.

611

612 3.4.6 Budget uncertainties

613 Estimates for Fe budgets are challenging and often contain large uncertainties. This is

614 primarily due to the lack of site- and time-specific flux data. Moreover, the mean annual

615 estimates, necessary for reliable supply calculations, reach a high level of accuracy only after

616 the same region has been monitored multiple times to cover seasonal and annual anomalies.

617 In the following, we will discuss the uncertainty of the different Fe fluxes in the blooming

618 region north of South Georgia.

619 We identified three main processes that account together for ~98% of the total Fe flux

620 in the blooming region, and thus contribute largest uncertainties; the horizontal flux, dry/wet

621 deposition, and winter entrainment. Horizontal flux estimates of this study rely on literature

622 values that were collected offshore the Antarctic Peninsula. In contrast, South Georgia is an

623 island with a confined shelf region and thus horizontal DFe fluxes may differ greatly.

624 Furthermore, we showed that dry deposition dust fluxes are generally low, but showed in

625 addition that the Fe flux can be supplemented strongly by sporadic wet deposition events (~

626 1.0 ± 1.2 µmol DFe m^{-2} d^{-1}) (Chance et al., 2015). Atmospheric fluxes are variable,

627 illustrated by the large standard deviation of the wet deposition Fe fluxes obtained at 40°S.

628 Furthermore, to determine the magnitude of the seasonal DFe winter entrainment reliable

629 estimates of the winter mixing layer depth (WMLD) and the ferrocline are required. Even

630 though the WMLD can be estimated very precisely using Argo float data, the depth of

631 ferrocline in the manuscript of Tagliabue et al. (2014) is based on 140 unique observations

632 distributed over the entire Southern Ocean. Due to this regional anomalies are not captured.

633 In addition to the DFe fluxes in the blooming region, we also assume that the biological Fe

634 demand estimated for the phytoplankton community contributes a large error. The biological

635 Fe requirements were determined using satellite derived net primary production data and an

636 average intracellular Fe/C ratio derived from 5 different diatom species native to the Southern

637 Ocean. Both parameters are not well constrained and because of the lack of observational

638 data we applied the lowest intracellular Fe/C ratio available in the literature (Strzepek et al.,

639 2011). However, we found that even small changes of the both parameters change the

640 estimated Fe availability in the bloom region strongly. Nevertheless, flux estimates even

641 with large uncertainties can help us understand the degree of the nutrient supply vs.

642 consumption by organisms and help to pinpoint the limitation of the estimates made. To

643 ultimately reduce the level of uncertainty and to improve our biogeochemical models more

644 observational data from the bloom region north of South Georgia is required.

645

646 **4. Conclusions**

647   Shelf sediment-derived Fe and Fe released from Antarctic krill significantly

648 contribute to the DFe distribution in the shelf waters around South Georgia. Nevertheless,

649 DFe enriched in shelf waters are not effectively advected to the phytoplankton bloom region

650 downstream of the island. Together with other Fe supplies, such as aeolian dust, deep winter

651 mixing and diapycnal mixing, the horizontal advection contributes only ~30% to the Fe

652 requirements of a phytoplankton bloom downstream of South Georgia. We therefore

653 hypothesize that the majority of the Fe is derived from remineralisation of Fe enriched

654 phytoplankton cells and biogenic particles that are transported with the water masses into the

655 bloom region.

656 While we highlight the importance of grazers and the cycling of various particulate Fe

657 phases in the Fe-fertilisation of the South Georgia bloom, more work is needed to clarify the

658 transport mechanisms of dissolved and particulate Fe.

659

660 **Author contribution**

661 CS, KS, EPA, SF, and AAt designed the experiments for JC247. CS, MDP and AAt

662 performed the sampling and krill incubation experiments during JC247. CS and MC analysed

663 the trace metal samples at NOCS. EPA sampled the seawater during JC274. Samples from

664 JC274 were analysed by CS and MC. AAq, WBH and RM designed the experiments for

665 JR55 and AAq analysed the samples. CS prepared the manuscript with contributions from all

666 co-authors.

667

References

Achterberg, E. P., Steigenberger, S., Marsay, C. M., LeMoigne, F. A. C., Painter, S. C.,

Baker, A. R., Connelly, D. P., Moore, C. M., Tagliabue, A., and Tanhua, T.: Iron

Biogeochemistry in the High Latitude North Atlantic Ocean, Scientific Reports, 8(1283), 1-

12, 2018.

Atkinson, A.: Diets and feeding selectivity among the epipelagic copepod community near

South Georgia in summer, Polar Biol., 14, 551-560, 1994.

Atkinson, A., Whitehouse, M. J., Priddle, J., Cripps, G. C., Ward, P., and Brandon, M. A.:

South Georgia, Antarctica: a productive, cold water, pelagic ecosystem, Mar. Ecol.-Prog.

Ser., 216, 279-308, 2001.

Berger, C. J. M., Lippiatt, S. M., Lawrence, M. G., and Bruland, K. W.: Application of a

chemical leach technique for estimating labile particulate aluminum, iron, and manganese in

the Columbia River plume and coastal waters off Oregon and Washington, J. Geophys. Res.,

113, 1-16, 2008.

Bonneville, S., Behrends, T., and Van Cappellen, P.: Solubility and dissimilatory reduction

kinetics of iron(III) oxyhydroxides: A linear free energy relationship, Geochim. Cosmochim.

Act., 73, 5273-5282, 2009.

Borrione, I., Aumont, O., Nielsdottir, M. C., and Schlitzer, R.: Sedimentary and atmospheric

sources of iron around South Georgia, Southern Ocean: a modelling perspective,

Biogeosciences Discuss., 10, 10811-10858, 2013.

Boudreau, B. P. and Scott, M. R.: A model for the diffusion-controlled growth of deep-sea

manganese nodules, Americ. J. Sc., 278, 903-929, 1978.

Boyd, P. W., Law, C. S., Hutchins, D. A., Abraham, E. R., Croot, P. L., Ellwood, M., Frew,

R. D., Hadfield, M., Hall, J., Handy, S., Hare, C., Higgins, J., Hill, P., Hunter, K. A.,

LeBlanc, K., Maldonado, M. T., McKay, R. M., Mioni, C., Oliver, M., Pickmere, S.,

700 Pinkerton, M., Safi, K., Sander, S., Sanudo-Wilhelmy, S. A., Smith, M., Strzepek, R., Tovar-

701 Sanchez, A., and Wilhelm, S. W.: FeCycle: Attempting an iron biogeochemical budget from

702 a mesoscale SF6 tracer experiment in unperturbed low iron waters, Global Biogeochem.

703 Cycles, 19, 1-13, 2005.

704 Boyd, P. W., Strzepek, R. F., Ellwood, M. J., Hutchins, D. A., Nodder, S. D., Twining, B. S.,

705 and Wilhelm, S. W.: Why are biotic iron pools uniform across high- and low-iron pelagic

706 ecosystems?, Global Biogeochem. Cycles, 29, 1028-1043, 2015.

707 Browning, T. J., Bouman, H. A., Henderson, G. M., Mather, T. A., Pyle, D. M., Schlosser,

708 C., Woodward, E. M. S., and Moore, C. M.: Strong responses of Southern Ocean

709 phytoplankton communities to volcanic ash, Geophys. Res. Lett., 41, 1-7, 2014.

710 Buesseler, K. O., Andrews, J. E., Pike, S. M., and Charette, M. A.: The Effects of Iron

711 Fertilization on Carbon Sequestration in the Southern Ocean, Science, 304, 414-417, 2004.

712 Canfield, D. E. and Thamdrup, B.: Towards a consistent classification scheme for

713 geochemical environments, or, why we wish the term 'suboxic' would go away, Geobiol., 7,

714 385-392, 2009.

715 Cassar, N., Bender, M. L., Barnett, B. A., Fan, S., Moxim, W. J., Levy II, H., and Tilbrook,

716 B.: The Southern Ocean Biological Response to Aelian Iron Input, Science, 317, 1067-1070,

717 2007.

718 Chance, R., Jickells, T. D., and Baker, A. R.: Atmospheric trace metal concentrations,

719 solubility and deposition fluxes in remote marine air over the south-east Atlantic, Mar.

720 Chem., 177, 45-55, 2015.

721 Charette, M. A., Gonneea, M. E., Morris, P., Statham, P., Fones, G., Planquette, H., Salter, I.,

722 and Garabato, A. N.: Radium isotopes as tracers of iron sources fueling a Southern Ocean

723 phytoplankton bloom, Deep-Sea Res. II, 54, 1989-1998, 2007.

724 Chase, Z., Hales, B., Cowles, T., Schwartz, R., and van Geen, A.: Distribution and variability

725 of iron input to Oregon coastal waters during the upwelling season, J. Geophys. Res., 110, 1-

726 14, 2005.

727 Chen, M. and Wang, W.-X.: Bioavailability of natural colloid-bound iron to marine plankton:

728 Influences of colloidal size and aging, Limnol. Oceanogr., 46, 1956-1967, 2001.

729 Conway, T. M., Wolff, E. W., Rothlisberger, R., Mulvaney, R., and Elderfield, H. E.:

730 Constraints on soluble aerosol iron flux to the Southern Ocean at the Last Glacial Maximum,

731 Nat. Commun., 6, 1-9, 2015.

732 de Boyer Montégut, C., Madec, G., Fischer, A. S., Lazar, A., and Iudicone, D.: Mixed layer

733 depth over the global ocean: An examination of profile data and a profile-based climatology,

734 J. Geophys. Res., 109, 1-20, 2004.

735 de Jong, J., Schoemann, V., Lannuzel, D., Croot, P., de Baar, H. J. W., and Tison, J. L.:

736 Natural iron fertilization of the Atlantic sector of the Southern Ocean by continental shelf

737 sources of the Antarctic Peninsula, J. Geophys. Res., 117, 1-25, 2012.

738 Fielding, S., Watkins, J. L., Trathan, P. N., Enderlein, P., Waluda, C. M., Stowasser, G.,

739 Tarling, G. A., and Murphy, E. J.: Interannual variability in Antarctic krill (Euphausia

740 superba) density at South Georgia, Southern Ocean: 1997–2013, ICES J. Mar. Sci., 2014. 1-

741 11, 2014.

742 Fitzsimmons, J. N. and Boyle, E. A.: Both soluble and colloidal iron phases control dissolved

743 iron variability in the tropical North Atlantic Ocean, Geochim. Cosmochim. Act., 125, 539-

744 550, 2014.

745 Gabric, A. J., Cropp, R. A., McTainsh, G. H., Johnston, B. M., Butler, H., Tilbrook, B., and

746 Keywood, M.: Australian dust storms in 2002 and 2003 and their impact on Southern Ocean

747 biogeochemistry, Global Biogeochem. Cycles, 24, 1-17, 2010.

748   Gao, Y., Kaufman, Y. J., Tanré, D., Kolber, D., and Falkowski, P. G.: Seasonal distributions

749   of aeolian iron fluxes to the global ocean, Geophys. Res. Lett., 28, 29-32, 2001.

750   Gassó, S. and Stein, A. F.: Does dust from Patagonia reach the sub-Antarctic Atlantic

751   Ocean?, Geophys. Res. Lett., 34, 1-5, 2007.

752   German, C. R., Casciotti, K. A., Dutay, J.-C., Heimbürger, L. E., Jenkins, W. J., Measures, C.

753   I., Mills, R. A., Obata, H., Schlitzer, R., Tagliabue, A., Turner, D. R., and Whitby, H.:

754   Hydrothermal impacts on trace element and isotope ocean biogeochemistry, Philos Trans A

755   Math Phys Eng Sci, 374, 1-19, 2016.

756   Gerringa, L. J. A., Alderkamp, A.-C., Laan, P., Thuróczy, C.-E., De Baar, H. J. W., Mills, M.

757   M., van Dijken, G. L., van Haren, H., and Arrigo, K. R.: Iron from melting glaciers fuels the

758   phytoplankton blooms in Amundsen Sea (Southern Ocean): Iron biogeochemistry, Deep-Sea

759   Res. II, 71-76, 16-31, 2012.

760   Giering, S. L. C., Steigenberger, S., Achterberg, E. P., Sanders, R., and Mayor, D. J.:

761   Elevated iron to nitrogen recycling by mesozooplankton in the Northeast Atlantic Ocean,

762   Geophys. Res. Lett., 39, L12608, 2012.

763   Gilpin, L. C., Priddle, J., Whitehouse, M. J., Savidge, G., and Atkinson, A.: Primary

764   production and carbon uptake dynamics in the vicinity of South Georgia-balancing carbon

765   fixation and removal, Mar. Ecol. Prog. Ser., 242, 51-62, 2002.

766   Hamm, C. E., Merkel, R., Springer, O., Jurkojc, P., Maier, C., Prechtel, K., and Smetacek, V.:

767   Architecture and material properties of diatom shells provide effective mechanical protection,

768   Nature, 421, 841-843, 2003.

769   Ho, T.-Y., Quigg, A., Finkel, Z. V., Milligan, A. J., Wyman, K., Falkowski, P. G., and Morel,

770   F. M. M.: The elemental composition of some marine phytoplankton, J. Phycol., 39, 1145-

771   1159, 2003.

772   Homoky, W. B., Hembury, D. J., Hepburn, L. E., Mills, R. A., Statham, P. J., Fones, G. R.,

773   and Palmer, M. R.: Iron and manganese diagenesis in deep sea volcanogenic sediments and

774   the origins of pore water colloids, Geochim. Cosmochim. Act., 75, 5032-5048, 2011.

775   Homoky, W. B., Severmann, S., McManus, J., Berelson, W. M., Riedel, T. E., Statham, P. J.,

776   and Mills, R. A.: Dissolved oxygen and suspended particles regulate the benthic flux of iron

777   from continental margins, Mar. Chem., 134–135, 59-70, 2012.

778   Homoky, W. B., Weber, T., Berelson, W. M., Conway, T. M., Henderson, G. M., van Hulten,

779   M., Jeandel, C., Severmann, S., and Tagliabue, A.: Quantifying trace element and isotope

780   fluxes at the ocean–sediment boundary: a review, Philos Trans A Math Phys Eng Sci, 374,

781   2016.

782   Hutchins, D. A. and Bruland, K. W.: Grazer-mediated regeneration and assimilation of Fe, Zn

783   and Mn from planktonic prey, Mar. Ecol.-Prog. Ser., 110, 259-269, 1994.

784   Iwade, S., Kuma, K., Isoda, Y., Yoshida, M., Kudo, I., Nishioka, J., and Suzuki, K.: Effect of

785   high iron concentrations on iron uptake and growth of a coastal diatom Chaetoceros sociale,

786   Aquat. Microb. Ecol., 43, 177-191, 2006.

787   Jones, E. M., Bakker, D. C. E., Venables, H. J., and Hardman-Mountford, N. J.: Seasonal

788   cycle of CO2 from the sea ice edge to island blooms in the Scotia Sea, Southern Ocean, Mar.

789   Chem., 177, 490-500, 2015.

790   Jones, E. M., Bakker, D. C. E., Venables, H. J., and Watson, A. J.: Dynamic seasonal cycling

791   of inorganic carbon downstream of South Georgia, Southern Ocean, Deep-Sea Res. II, 59–60,

792   25-35, 2012.

793   Kalnejais, L. H., Martin, W. R., and Bothner, M. H.: The release of dissolved nutrients and

794   metals from coastal sediments due to resuspension, Mar. Chem., 121, 224-235, 2010.

795   Klar, J. K., Homoky, W. B., Statham, P. J., Birchill, A. J., Harris, E. L., Woodward, E. M. S.,

796   Silburn, B., Cooper, M. J., James, R. H., Connelly, D. P., Chever, F., Lichtschlag, A., and

797   Graves, C.: Stability of dissolved and soluble Fe(II) in shelf sediment pore waters and release

798   to an oxic water column, Biogeochemistry, 2017. 1-19, 2017.

799   Korb, R. E., Whitehouse, M. J., and Ward, P.: SeaWiFS in the southern ocean: spatial and

800   temporal variability in phytoplankton biomass around South Georgia, Deep-Sea Res. II, 51,

801   99-116, 2004.

802   Koschinsky, A., Winkler, A., and Fritsche, U.: Importance of different types of marine

803   particles for the scavenging of heavy metals in the deep-sea bottom water, Appl Geochem,

804   18, 693-710, 2003.

805   Kurapov, A. L., Allen, J. S., and Egbert, G. D.: Combined Effects of Wind-Driven Upwelling

806   and Internal Tide on the Continental Shelf, Journal of Physical Oceanography, 40, 737-756,

807   2010.

808   Lam, P. J. and Bishop, J. K. B.: The continental margin is a key source of iron to the HNLC

809   North Pacific Ocean, Geophys. Res. Lett., 35, 1-5, 2008.

810   Liu, X. and Millero, F. J.: The solubility of iron in seawater, Mar. Chem., 77, 43-54, 2002.

811   Ma, S., Tao, Z., Yang, X., Yu, Y., Zhou, X., M, W., and Li, Z.: Estimation of marine primary

812   productivity from satellite-derived phytoplankton absorption data, IEEE J-STARS, 7, 3084-

813   3092, 2014.

814   Marchetti, A., Parker, M. S., Moccia, L. P., Lin, E. O., Arrieta, A. L., Ribalet, F., Murphy, M.

815   E. P., Maldonado, M. T., and Armbrust, E. V.: Ferritin is used for iron storage in bloom-

816   forming marine pennate diatoms, Nature, 457, 467-470, 2009.

817   Marsay, C. M., Sedwick, P. N., Dinniman, M. S., Barrett, P. M., Mack, S. L., and

818   McGillicuddy, D. J.: Estimating the benthic efflux of dissolved iron on the Ross Sea

819   continental shelf, Geophys. Res. Lett., 41, 7576-7583, 2014.

820   Meredith, M. P., Brandon, M. A., Murphy, E. J., Trathan, P. N., Thorpe, S. E., Bone, D. G.,

821   Chernyshkov, P. P., and Sushin, V. A.: Variability in hydrographic conditions to the east and

822   northwest of South Georgia, 1996–2001, J. Marine Syst., 53, 143-167, 2005.

823   Milne, A., Schlosser, C., Wake, B. D., Achterberg, E. P., Chance, R., Baker, A. R., Forryan,

824   A., and Lohan, M. C.: Particulate phases are key in controlling dissolved iron concentrations

825   in the (sub)tropical North Atlantic, Geophys. Res. Lett., 44, 2377-2387, 2017.

826   Moore, W. S.: Determining coastal mixing rates using radium isotopes, Cont. Shelf Res., 20,

827   1993-2007, 2000.

828   Murphy, E. J., Trathan, P. N., Watkins, J. L., Reid, K., Meredith, M. P., Forcada, J., Thorpe,

829   S. E., Johnston, N. M., and Rothery, P.: Climatically driven fluctuations in Southern Ocean

830   ecosystems, P ROY SOC B-BIOL SCI, 274, 3057-3067, 2007.

831   Nielsdóttir, M. C., Bibby, T. S., Moore, C. M., Hinz, D. J., Sanders, R., Whitehouse, M.,

832   Korb, R., and Achterberg, E. P.: Seasonal and spatial dynamics of iron availability in the

833   Scotia Sea, Mar. Chem., 130–131, 62-72, 2012.

834   Pakhomova, S. V., Hall, P. O. J., Kononets, M. Y., Rozanov, A. G., Tengberg, A., and

835   Vershinin, A. V.: Fluxes of iron and manganese across the sediment–water interface under

836   various redox conditions, Mar. Chem., 107, 319-331, 2007.

837   Planquette, H., Sanders, R., Statham, P. J., Morris, P. J., and Fones, G. R.: Fluxes of

838   particulate iron from the upper ocean around the Crozet Islands: A naturally iron-fertilized

839   environment in the Southern Ocean, Global Biogeochem. Cycles, 25, 1-12, 2011.

840   Planquette, H., Statham, P. J., Fones, G. R., Charette, M. A., Moore, C. M., Salter, I.,

841   Nedelec, F. H., Taylor, S. L., French, M., Baker, A. R., Mahowald, N., and Jickells, T. D.:

842   Dissolved iron in the vicinity of the Crozet Islands, Southern Ocean, Deep-Sea Res. II, 54,

843   1999-2019, 2007.

844   Pollard, R. T., Salter, I., Sanders, R. J., Lucas, M. I., Moore, C. M., Mills, R. A., Statham, P.

845   J., Allen, J. T., Baker, A. R., Bakker, D. C. E., Charette, M. A., Fielding, S., Fones, G. R.,

846   French, M., Hickman, A. E., Holland, R. J., Hughes, J. A., Jickells, T. D., Lampitt, R. S.,

847   Morris, P. J., Nedelec, F. H., Nielsdottir, M., Planquette, H., Popova, E. E., Poulton, A. J.,

848   Read, J. F., Seeyave, S., Smith, T., Stinchcombe, M., Taylor, S., Thomalla, S., Venables, H.

849   J., Williamson, R., and Zubkov, M. V.: Southern Ocean deep-water carbon export enhanced

850   by natural iron fertilization, Nature, 457, 577-580, 2009.

851   Raiswell, R., Benning, L. G., Tranter, M., and Tulaczyk, S.: Bioavailable iron in the Southern

852   Ocean: the significance of the iceberg conveyor belt, Geochemical Transactions, 9, 1-9, 2008.

853   Raiswell, R. and Canfield, D. E.: The Iron Biogeochemical Cycle Past and Present,

854   Geochemical Perspectives, 1, 1-2, 2012.

855   Rapp, I., Schlosser, C., Rusiecka, D., Gledhill, M., and Achterberg, E. P.: Automated

856   preconcentration of Fe, Zn, Cu, Ni, Cd, Pb, Co, and Mn in seawater with analysis using high-

857   resolution sector field inductively-coupled plasma mass spectrometry, Anal. Chimi. Acta,

858   976, 1-13, 2017.

859   Ratnarajah, L., Lannuzel, D., Townsend, A. T., Meiners, K. M., Nicol, S., Friedlaender, A.

860   S., and Bowie, A. R.: Physical speciation and solubility of iron from baleen whale faecal

861   material, Mar. Chem., 2017. 2017.

862   Sato, M., Takeda, S., and Furuya, K.: Iron regeneration and organic iron(III)-binding ligand

863   production during in situ zooplankton grazing experiment, Mar. Chem., 106, 471-488, 2007.

864   Schlosser, C., De La Rocha, C. L., and Croot, P. L.: Effects of iron surface adsorption and

865   sample handling on iron solubility measurements, Mar. Chem., 127, 48-55, 2011.

866   Schmidt, K., Atkinson, A., Steigenberger, S., Fielding, S., Lindsay, M. C. M., Pond, D. W.,

867   Tarling, G. A., Klevjer, T. A., Allen, C. S., Nicol, S., and Achterberg, E. P.: Seabed foreaging

868   by Antarctic krill: Implications for stock assessment, bentho-pelagic coupling, and the

869   vertical transfer of iron, Limnol. Oceanogr., 56, 1411-1428, 2011.

870   Schmidt, K., Schlosser, C., Atkinson, A., Fielding, S., Venables, H. J., Waluda, C. M., and

871   Achterberg, E. P.: Zooplankton gut passage mobilises lithogenic iron for ocean productivity,

872   Curr. Biol., 26, 1-7, 2016.

873   Strzepek, R., Maldonado, M. T., Hunter, K. A., Frew, R. D., and Boyd, P. W.: Adaptive

874   strategies by Southern Ocean phytoplankton to lessen iron limitation: Uptake of organically

875   complexed iron and reduced cellular iron requirements, Limnol. Oceanogr., 56, 1983-2002,

876   2011.

877   Tagliabue, A., Sallee, J.-B., Bowie, A. R., Levy, M., Swart, S., and Boyd, P. W.: Surface-

878   water iron supplies in the Southern Ocean sustained by deep winter mixing, Nat Geosci, 7,

879   314-320, 2014.

880   Tsuda, A., Saito, H., Machida, R. J., and Shimode, S.: Meso- and microzooplankton

881   responses to an in situ iron fertilization experiment (SEEDS II) in the northwest subarctic

882   Pacific, Deep-Sea Res. II, 56, 2767-2778, 2009.

883   Wedepohl, K. H.: The composition of the continental crust, Geochim. Cosmochim. Act., 59,

884   1217-1232, 1995.

885   Wells, M. L., Mayer, L. M., Donard, O. F. X., Sierra, M. M. D., and Ackelson, S. G.: The

886   Photolysis Of Colloidal Iron In The Oceans, Nature, 353, 248-250, 1991.

887   Whitehouse, M. J., Korb, R. E., Atkinson, A., Thorpe, S. E., and Gordon, M.: Formation,

888   transport and decay of an intense phytoplankton bloom within the High-Nutrient Low-

889   Chlorophyll belt of the Southern Ocean, J. Marine Syst., 70, 150-167, 2008.

890   Wing, S. R., Jack, L., Shatova, O., Leichter, J. J., Barr, D., Frew R. D., and Gault-Ringold,

891   M.: Seabirds and marine mammals redistribute bioavailable iron in the Southern Ocean, Mar.

892   Ecol. Prog. Ser., 510, 1-13, 2014.

893   Wolanski, E. J. and Delesalle, B.: Upwelling by internal waves, Tahiti, French Polynesia,

894   Cont. Shelf Res., 15, 357-368, 1995.

895   Yoshida, M., Kuma, K., Iwade, S., Isoda, Y., Takata, H., and Yamada, M.: Effect of aging

896   time on the availability of freshly precipitated ferric hydroxide to costal marine diatoms, Mar.

897   Biol., 149, 379-392, 2006.

898

Table 1: OTE-seawater samples: Fe, Mn, and Al concentrations determined for the dissolved (D) (0.2 μm) and the leachable particulate fraction (LP$_{UN}$) (total dissolvable – dissolved) of unfiltered seawater samples collected during JR247. Additional information covers sampling date, site (station) ID, event number and latitude + longitude.

Date	Site ID	Depth	Leach. Part. (nmol L^{-1})			Dissolved (nmol L^{-1})		
	Lat. & Lon.	(m)	LP$_{Un}$Fe	LP$_{Un}$Mn	LP$_{Un}$Al	DFe	DMn	DAl
04/01/2011	#9/10 (E95 & E97)	20	20.36	0.95	46.41	5.71	1.83	1.11
		50	15.18	0.42	40.86	3.19	1.88	2.27
	54.26°S, 35.35°W	100	9.86	0.23	20.43	1.55	0.92	2.07
		130	23.33	0.73	48.91	2.82	0.87	2.68
		150	23.71	0.43	46.95	2.35	1.03	0.12
		200	27.37	0.62	54.41	2.70	0.89	2.37
05/01/2011	#11/12 (E98 & E101)	20	4.05	0.38	6.68	2.19	0.41	3.57
		35	1.52	0.39	7.28	0.41	0.37	-
	54.62°S, 34.81°W	50	9.30	0.60	22.20	7.18	0.64	13.31
		75	1.28	0.31	7.85	0.77	0.35	4.56
		100	2.02	0.32	3.34	1.09	0.35	1.47
		150	1.55	0.38	3.18	1.10	0.45	-
		200	13.10	1.31	23.81	1.26	1.17	3.07
		300	8.62	0.70	23.25	1.06	0.55	-
		400	8.81	0.54	16.54	2.05	0.46	2.69
		500	4.51	0.41	11.41	0.72	0.38	0.76
		600	2.75	0.37	10.32	0.96	0.36	0.77
		700	4.81	0.41	16.85	0.82	0.35	-
06/01/2011	#13 (E105)	20	3.46	0.62	14.68	0.28	0.57	4.53
		35	1.00	0.33	7.17	0.10	0.28	2.64
	54.53°S, 35.27°W	50	7.09	0.71	22.62	1.26	0.57	5.77
		75	25.03	1.09	61.94	1.23	0.64	5.86
		100	34.06	1.30	87.43	0.82	0.74	4.08
07/01/2011	#14 (E113)	20	4.00	0.89	7.87	0.64	0.85	2.57
		50	2.23	0.31	7.64	0.27	0.32	1.80
	54.56°S, 35.59°W	75	2.30	0.43	3.58	0.62	0.46	2.42
		100	2.26	0.44	3.34	0.35	0.46	0.46
		150	23.50	0.94	33.35	0.70	0.62	0.23
		200	82.26	2.12	103.11	2.69	0.77	2.31
08/01/2011	#15/16 (E119 & E129)	20	17.66	0.46	26.66	0.99	1.36	-
		35	16.60	0.30	13.37	0.96	1.27	-
	53.62°S, 36.34°W	50	16.30	0.23	18.49	1.21	1.40	-
		75	23.82	0.56	29.86	0.98	1.28	-
		100	8.49	0.10	10.50	0.73	0.56	-
		150	1.88	0.03	4.49	2.25	0.40	-
		200	2.72	0.02	1.40	0.63	0.44	2.87

		300	2.56	0.05	2.40	0.34	0.25	-
		400	3.75	0.02	5.28	0.48	0.30	1.17
		500	5.28	0.08	9.22	0.43	0.30	-
		600	5.50	0.09	11.45	0.53	0.28	1.63
		750	5.27	0.06	8.16	0.44	0.30	-
10/01/2011	#17 (E133)	20	10.92	0.22	7.43	2.31	1.20	3.76
		35	20.83	0.53	16.22	1.81	1.34	2.56
	53.90°S, 36.57°W	50	34.59	1.00	57.55	2.29	1.42	2.33
		75	118.25	2.18	64.36	4.21	1.86	2.19
		100	50.71	1.00	77.52	2.48	1.42	1.62
		150	112.28	2.23	86.09	3.39	1.41	0.86
11/01/2011	#18 (E138)	20	106.71	1.77	95.17	2.75	1.57	3.36
		35	83.53	0.00	100.32	1.97	1.33	2.44
	54.10°S, 36.25°W	50	9.67	0.00	18.23	0.74	0.85	-
		75	5.65	0.00	8.90	0.62	0.65	-
		100	4.50	0.08	23.65	1.25	0.48	5.18
		150	7.81	0.11	12.87	1.43	0.49	8.19
12/01/2011	#19/20 (E141 & E143)	20	60.19	2.11	54.29	1.46	1.71	5.30
		35	60.17	2.19	87.17	1.34	1.90	8.22
	53.54°S, 38.11°W	50	66.78	2.74	141.75	1.57	1.90	8.73
		75	71.69	1.78	79.19	1.61	2.13	11.45
		100	10.77	0.25	32.12	0.99	0.67	10.74
		150	5.43	0.13	31.35	1.84	0.92	12.00
		200	7.92	0.14	27.42	1.45	0.60	9.60
		400	5.35	0.00	23.61	1.61	0.45	18.44
		600	5.81	0.10	35.99	1.06	0.38	10.74
		800	4.26	0.13	35.67	1.07	0.36	11.95
13/01/2011	#21 (E151)	20	44.75	1.54	114.13	0.72	1.38	2.58
		35	39.99	1.82	73.37	0.77	0.94	2.29
	53.75°S, 38.98°W	50	48.57	2.03	94.66	1.24	1.36	1.91
		75	25.63	0.91	68.56	0.98	1.17	-
		100	64.06	1.91	114.03	2.33	1.32	1.51
		150	73.04	1.59	62.83	7.70	1.28	12.20

903

Table 2: SAPS samples: The particulate Fe (PFe), Mn (PMn), and Al (PAl) concentrations

in the top 150 m of the water column at the 14 sites visited during JR247. The particulate

fraction, P, is the sum of leachable (L) and refractory (R). Because of low concentrations, the

leachable fraction is indicated in percent of the P fraction. Additional information covers

sampling date, site (station) ID, event number, latitude and longitude, and water column

depth. (Depths marked by * indicate that the polycarbonate filter was corrupted after

retrieving the SAPS)

Date	Site ID	Depth	Particulate (nmol L^{-1})				Leach. Part. (% of P)	
	Lat. & Lon.	(m)	PFe	PMn	PAl	LFe	LMn	LAl
25/12/2010	#1/2 (E22)	20	5.17	0.08	4.82	0.37	2.39	1.65
	53.70°S, 38.21°W	50*	9.12	0.14	7.91	0.27	2.61	1.47
	(322 m)	150*	76.61	1.09	66.91	6.26	2.74	4.65
26/12/2010	#3 (E31)	20	6.62	0.09	6.64	0.02	3.30	0.79
	53.85°S, 39.14°W	50	267.48	3.85	162.59	1.48	0.79	0.65
	(287 m)	150	4.36	0.06	4.26	0.07	1.55	1.93
31/12/2010	#4/5 (E72)	20	8.52	0.12	7.99	0.51	1.68	2.62
	53.49°S, 37.71°W	50	15.15	0.23	12.96	0.56	2.44	2.74
	(1917 m)	150	2.33	0.03	2.15	0.65	1.78	2.42
02/01/2011	#6 (E80)	20	85.74	1.11	59.05	1.60	2.28	4.50
	53.99°S, 36.37°W	50	17.76	0.24	8.87	-	-	-
	(208 m)	150	137.39	2.02	98.54	3.46	0.91	2.81
03/01/2011	#7/8 (E88)	20	1.95	0.02	0.87	0.13	2.97	4.99
	54.10°S, 35.46°W	50	1.67	0.02	0.92	0.08	4.35	4.24
	(330 m)	150	1.23	0.02	0.71	0.19	2.11	5.13
04/01/2011	#9/10 (E96)	20	20.91	0.08	15.74	0.56	5.01	3.24
	54.26°S, 35.35°W	50	19.16	0.27	15.58	0.45	1.22	2.51
	(263 m)	150	54.06	0.77	48.10	1.08	1.65	2.08
05/01/2011	#11/12 (E100)	20*	1.49	0.01	0.86	0.18	4.42	2.92
	54.62°S, 34.81°W	50	0.87	0.01	0.60	0.27	6.63	4.20
	(747 m)	150	1.76	0.03	1.08	0.37	4.38	3.33
06/01/2011	#13 (E106)	20	2.75	0.03	1.78	0.63	3.13	4.29
	54.53°S, 35.27°W	50	4.11	0.05	3.07	0.44	2.04	2.76
	(133 m)	100	10.28	0.15	7.62	0.46	1.70	2.54
07/01/2011	#14 (E114)	20	2.80	0.04	1.84	0.07	1.58	3.29
	54.56°S, 35.59°W	50	1.41	0.02	0.97	0.10	2.57	3.92
	(263 m)	150	31.34	0.46	26.92	0.72	1.57	2.28
08/01/2011	#15/16 (E120)	20	24.54	0.37	22.91	0.85	3.95	1.88
	53.62°S, 36.34°W	50	27.72	0.40	23.23	0.43	3.65	1.36
	(852 m)	150	4.74	0.07	3.94	0.90	4.31	1.06

Date	Station	Depth					
10/01/2011	#17 (E134)	20	10.43	0.14	8.09	0.34	1.66	2.41
	53.90°S, 36.57°W	50	43.04	0.60	38.79	1.34	1.07	1.67
	(209 m)	150	207.48	3.10	194.88	1.72	0.82	1.50
11/01/2011	#18 (E139)	20	95.52	1.32	88.39	1.39	1.82	1.93
	54.10°S, 36.25°W	50	37.43	0.52	35.33	1.16	1.29	1.85
	(276 m)	150	28.00	0.41	23.60	1.26	2.35	2.27
12/01/2011	#19/20 (E142)	20	97.60	1.52	97.10	0.16	1.66	0.33
	53.54°S, 38.11°W	50	90.96	1.42	92.89	0.39	1.98	0.80
	(1741 m)	150	7.41	0.12	6.37	0.74	8.25	2.75
13/01/2011	#21 (E152)	20	50.75	0.85	52.78	0.06	2.99	0.12
	53.75°S, 38.98°W	50	59.59	0.93	59.98	0.05	2.15	0.09
	(269 m)	150	153.48	2.34	89.63	3.14	1.10	2.94

911

912 **Table 3:** Illustrates the different elemental ratios of earth crust, sediment, suspended (SAPS),

913 faecal pellet, and biogenic particles (average phytoplankton species).

particle	Fe/Mn (mol mol^{-1})	Fe/Al (mol mol^{-1})	Mn/Al (mol mol^{-1})	source
crustal	58.00	0.20	0.0035	a
sediment	51.50	0.34	0.0066	This study
suspended (SAPS)	68.00	1.25	0.0171	This study
faecal pellet	70.65	0.48	0.0069	This study
phytoplankton	1.70	-	-	b

914   a) Wedepohl, 1995; b) Ho et al., 2003

915

916 **Table 4: Sediment core samples:** Particulate iron (SFe), aluminum (SAl), and manganese

917 (SMn) concentrations in shelf sediments collected during JC055 in January and February

918 2011. Pore water data retrieved additionally from these three cores are listed for Fe (Fe$_{PW}$)

919 and Mn (Mn$_{PW}$). Additional information are event number (MC…), latitude + longitude, and

920 water column depth.

Station ID Lat. & Lon.	Depth (cm)	SFe (mol kg-1)	SAl (mol kg-1)	SMn (mmol kg-1)	Fe$_{PW}$ (µmol kg-1)	Mn$_{PW}$ (µmol kg-1)
#S1 (MC33)	0.5	0.58	1.77	11.56	3.01	2.29
54.16°S, 37.98°W	1.5	0.61	1.74	11.52	17.47	0.84
(257 m)	2.5	0.59	1.77	11.78	110.90	0.28
	3.5	0.6	1.86	12.05	106.24	0.53
	4.5	0.58	1.72	11.82	94.09	0.34
	5.5	0.59	1.86	12.04	82.79	0.27
	9	0.56	1.72	11.19	32.98	0.00
	15	0.55	1.74	11.15	2.44	0.06
	25	0.53	1.6	10.81	0.80	0.16
#S2 (MC34)	0.5	0.64	1.77	11.42	1.53	0.87
54.16°S, 37.94°W	1.5	0.6	1.79	11.73	/	/
(247 m)	2.5	0.58	1.76	11.81	0.97	0.24
	6.5	0.59	1.83	12.23	11.19	0.26
	10.5	0.58	1.8	11.78	14.28	0.25
	14.5	0.54	1.6	10.83	3.59	0.33
	16.5	0.56	1.72	11.22	2.27	0.31
#S3 (MC35)	0.5	0.61	1.67	11.42	1.46	0.43
54.15°S, 37.97°W	1.5	0.59	1.76	11.7	28.94	0.35
(254 m)	2.5	0.58	1.76	11.7	91.52	0.37
	3.5	0.59	1.81	12.03	40.16	0.44

5.5	0.57	1.78	11.58	49.37	0.56
8.5	0.59	1.82	11.65	67.92	0.52
17	0.54	1.69	10.8	3.87	0.34
19	0.55	1.67	10.86	1.82	0.12
25	0.55	1.77	11.19	2.73	0.36
29	0.56	1.79	11.19	5.64	0.16

921

922   **Table 5: Krill faecal pellets:** Particulate (P) and leachable (L) concentrations for Fe, Mn,

923   and Al determined for the 27 individual krill faecal pellet samples collected during 9 krill

924   incubation experiments on-board RRS *James Clark Ross* (JR247). The particulate fraction, P,

925   is the sum of leachable (L) and refractory (R). Because of low concentrations, the leachable

926   fraction is indicated in percent of the P fraction.

| # Sample	pellet weight (mg)	PFe (μg mg^{-1})	PAl (μg mg^{-1})	PMn (ng mg^{-1})	LFe (%)	LAl (%)	LMn (%)
1	4.87	0.88	1.06	12.5	6.33	8.83	13.24
2	2.18	1.33	1.68	16.7	3.02	8.81	8.22
3	4.26	1.07	1.90	17.8	5.37	3.27	11.81
4	1.91	5.19	5.53	76.1	2.15	1.95	5.68
5	1.41	2.70	2.84	39.1	2.46	1.59	3.54
7	7.80	67.1	64.2	998.3	2.93	2.21	3.25
8	0.99	2.71	2.42	35.0	3.76	4.59	5.99
10	1.48	6.42	4.89	71.6	0.29	4.83	0.91
13	2.79	4.13	3.11	50.3	0.36	5.07	1.53
15	0.77	37.3	38.1	531.1	2.03	2.80	6.21
16	1.21	6.35	6.22	81.2	1.24	7.47	3.13
18	12.27	40.0	36.6	582.5	3.95	2.07	4.29
19	2.19	11.2	9.49	146.9	0.15	2.03	1.07
22	2.43	48.1	49.7	721.5	0.81	2.32	0.98
40	3.35	22.8	22.0	337.4	5.51	3.21	5.50
41	8.55	6.91	7.14	103.1	1.11	1.88	4.31
42	3.5	25.7	24.8	376.2	5.09	2.98	5.29
45	0.40	3.96	4.43	43.3	1.27	13.90	1.46
47	7.65	3.63	3.92	52.7	0.34	0.68	3.65
48	0.63	3.06	3.21	34.1	0.05	4.22	0.76
49	4.42	29.6	28.5	438.4	1.65	2.93	1.95
50	7.46	2.31	2.37	34.6	0.36	0.51	2.78
51	5.18	28.0	27.1	431.3	1.85	2.60	2.01
62	1.20	4.63	4.68	68.0	0.31	1.78	0.47
68	2.25	44.0	40.2	667.4	4.84	1.95	4.77
69	1.66	43.6	44.8	663.7	5.66	2.13	5.46
71	3.47	35.3	36.4	557.7	1.50	1.99	1.76

927

928
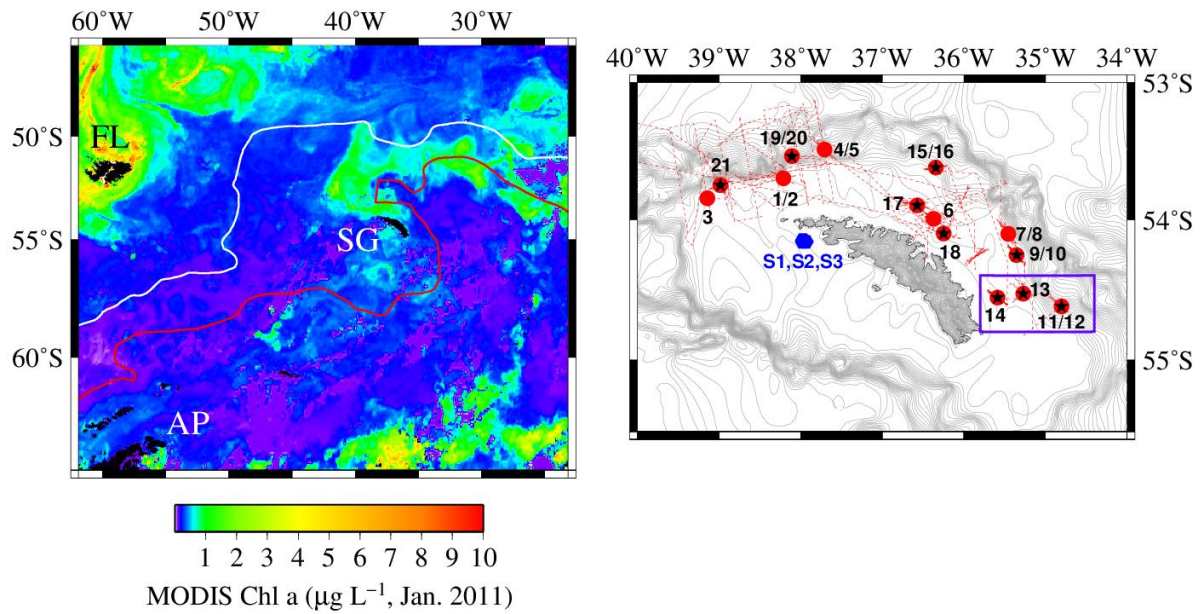
Figure 1: (Left figure) Locations of Falkland Islands (FL), South Georgia (SG), and Antarctic Peninsula (AP) in the Atlantic sector of the Southern Ocean. South Georgia is located between the Antarctic Polar Front (PF, white line) and the Subantarctic Circumpolar Current Front (SACCF, red line). The colour bar represents the Chlorophyll a (Chl a) content recorded by the MODIS satellite in January 2011. (Right figure) The region around SG and the **OTE** (black stars) and **SAPS** sampling sites (red points) visited during JR247. The red dashed line illustrates the cruise track of JR247. The three sediment sampling sites S1, S2, and S3 visited during JC055 are shown by blue hexagons. The purple box indicates the W-E transect from shelf site #14 via site #13 to the shelf edge site #11/12. The ocean bathymetry of the region was plotted using the GEBCO bathymetric data set. The shelf of South Georgia is between 100 and 250 m deep and extends about 30 to 100 km (shelf edge indicated by high density of isobaths).
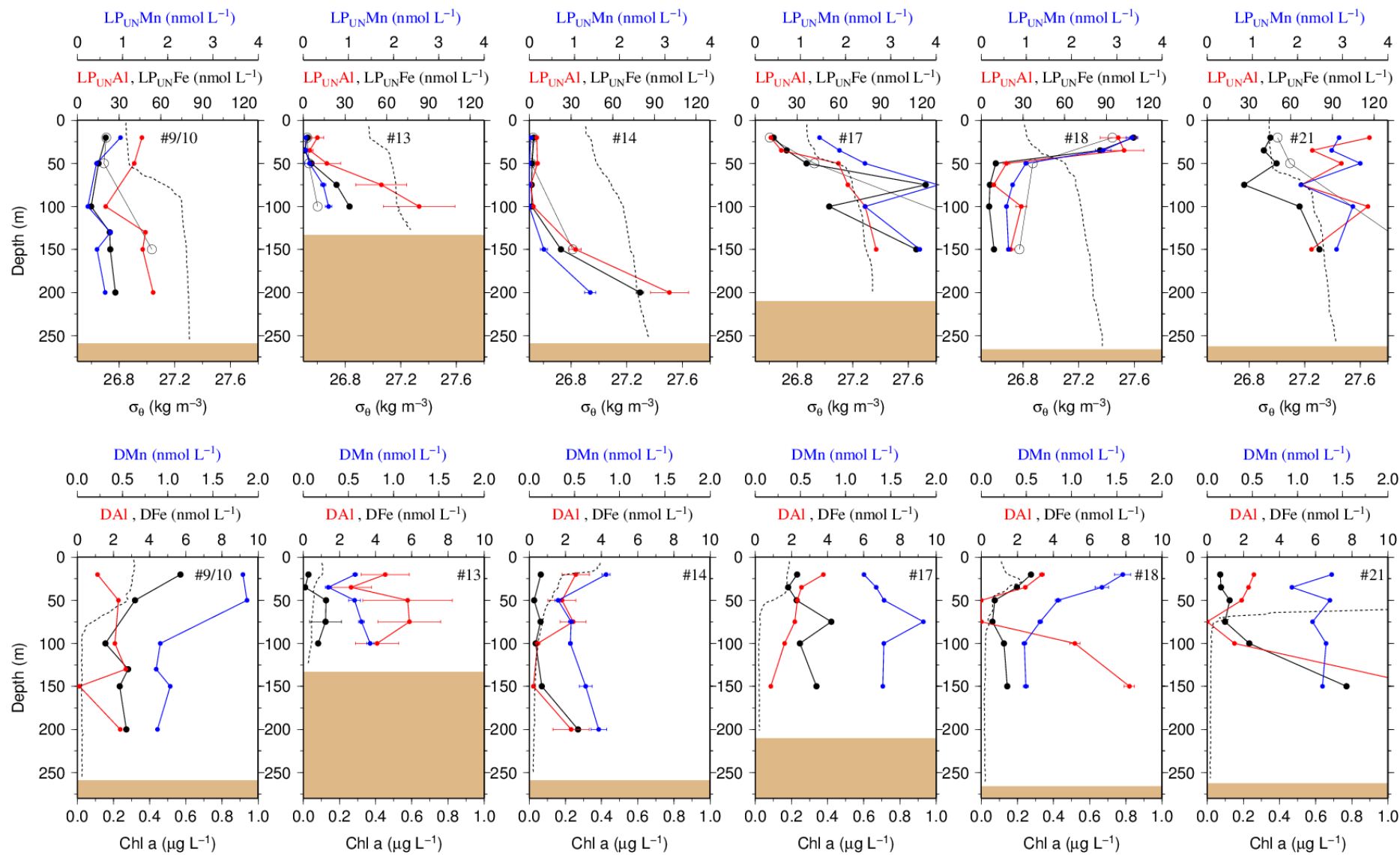
942   **Figure 2:** (Upper row) **OTE-seawater samples:** Distribution of leachable particulate iron

943   ($LP_{Un}Fe$ in black), manganese ($LP_{Un}Mn$ in blue), and aluminium ($LP_{Un}Al$ in red)

944   concentrations in the water column of stations located on the island shelf (125 m – 270 m

945   water depth). **SAPS samples:** The particulate Fe (PFe) fraction retrieved by SAPS is

946   illustrated with open black circles and corresponds to the same axis as $LP_{Un}Fe$.

947   Concentrations above 120 nmol L^{-1} are listed in Table 1 and 2. Error bars represent the

948   standard deviation of the analysis.   Density sigma-theta (σ_θ) in kg m^{-3} is illustrated by the

949   black dashed line. (Lower row) **OTE-seawater samples:** Dissolved iron (DFe), manganese

950   (DMn), and aluminium (DAl) are represented by the same colour code as above. Dashed

951   lines illustrate Chlorophyll a (Chl a) content of the water column recorded by the CTD

952   fluorometer.
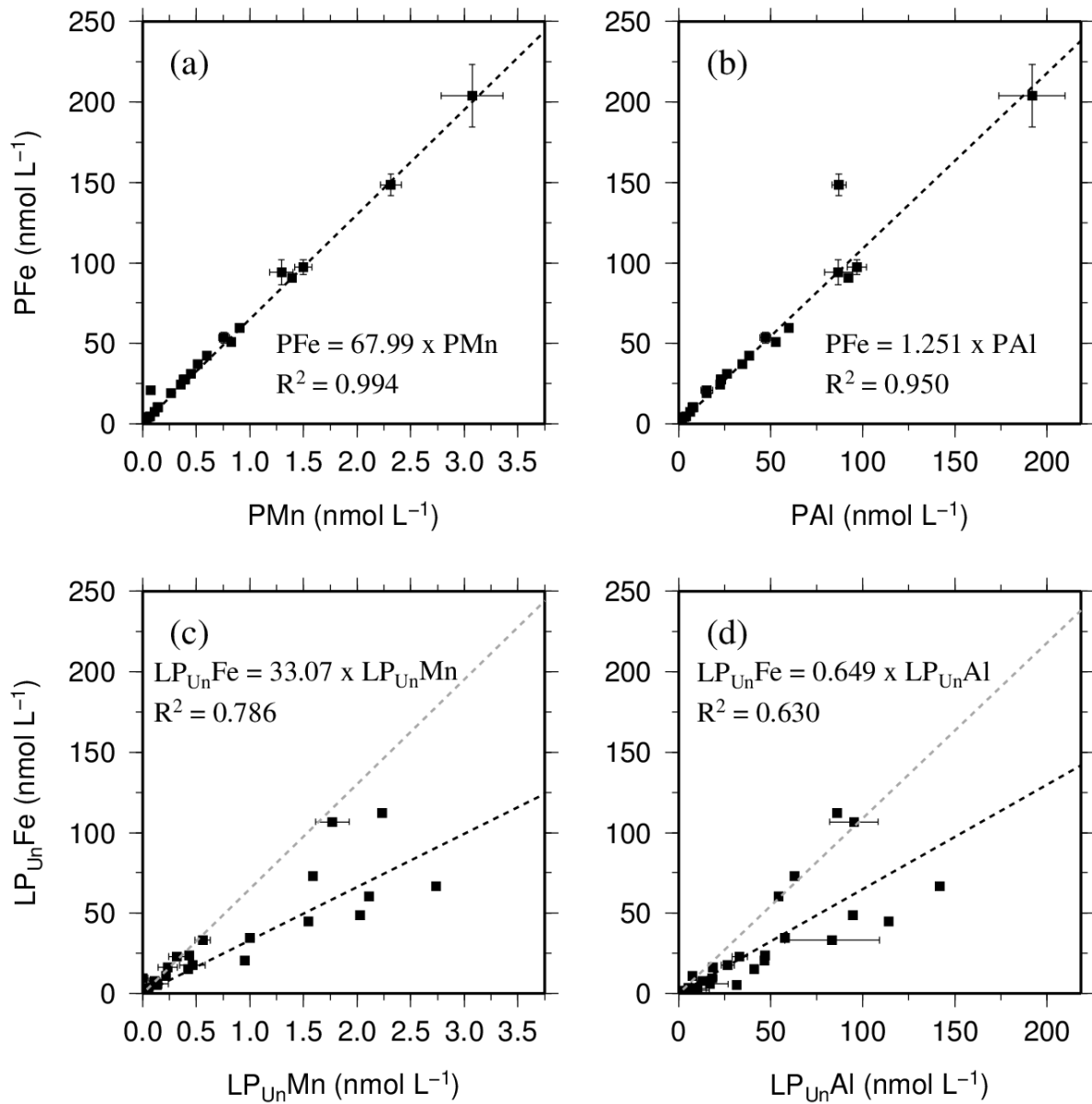
Figure 3: Relationship of the entire data set for the particulate fraction of Fe, Mn, and Al in particulates (P) retrieved using SAPS ((a) and (b)) and the leachable particulate fraction (LP_{UN}) estimated from unfiltered and dissolved seawater samples collected using OTE bottles ((c) and (d)). Error bars represent the standard deviation of the analysis. The linear regression of each relationship is illustrated by a dashed black line, the formula, and the R^2. The grey dashed line in c. and d. represents the linear relationship of particulate trace meals (P) shown in (a) and (b).

961
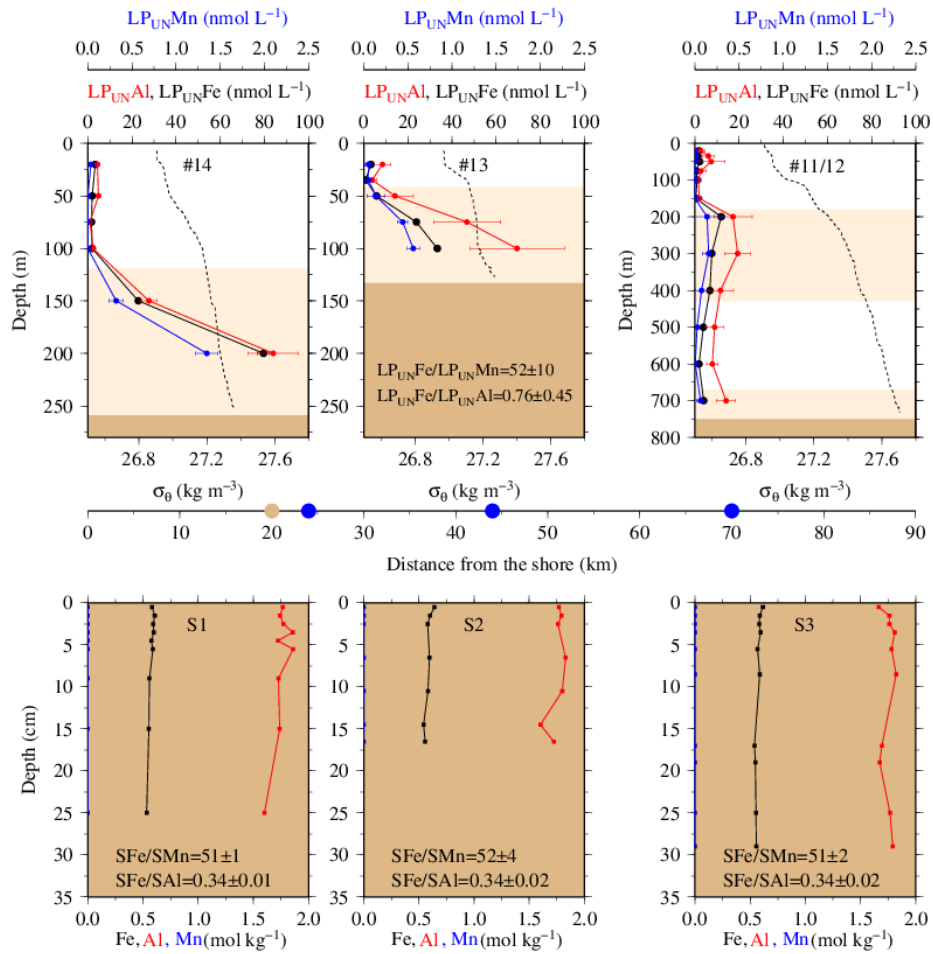
Figure 4: (Upper row) **OTE-seawater samples:** From left to right, concentrations of

leachable particulate iron (LP$_{Un}$Fe), aluminium (LP$_{Un}$Al), and manganese (LP$_{Un}$Mn) of

unfiltered seawater samples for the two shelf sites #14, #13 and the shelf edge site #11/12

(Note different depth scaling). Error bars represent the standard deviation of the analysis.

Water density (sigma-theta (σ_θ)) is shown by the dashed black line. Brown areas represent

sediments and pink areas the zone of resuspended sediment particles in the water column.

Diagram 14 (left) contains the average LP$_{Un}$Fe/LP$_{Un}$Al and LP$_{Un}$Fe/LP$_{Un}$Mn ratio of particles

in seawater samples collected within the pink layers. (Lower row) **Sediment core samples:**

Diagram S1, S2 and, S3 displays the Fe, Mn, and Al content in the three sediment cores.

Shown are average SFe/SAl and SFe/SMn ratios (mol/mol) of particles from the surface layer

for site S1, S2, and S3. Dots on the distance scaling in the middle represent the distance of

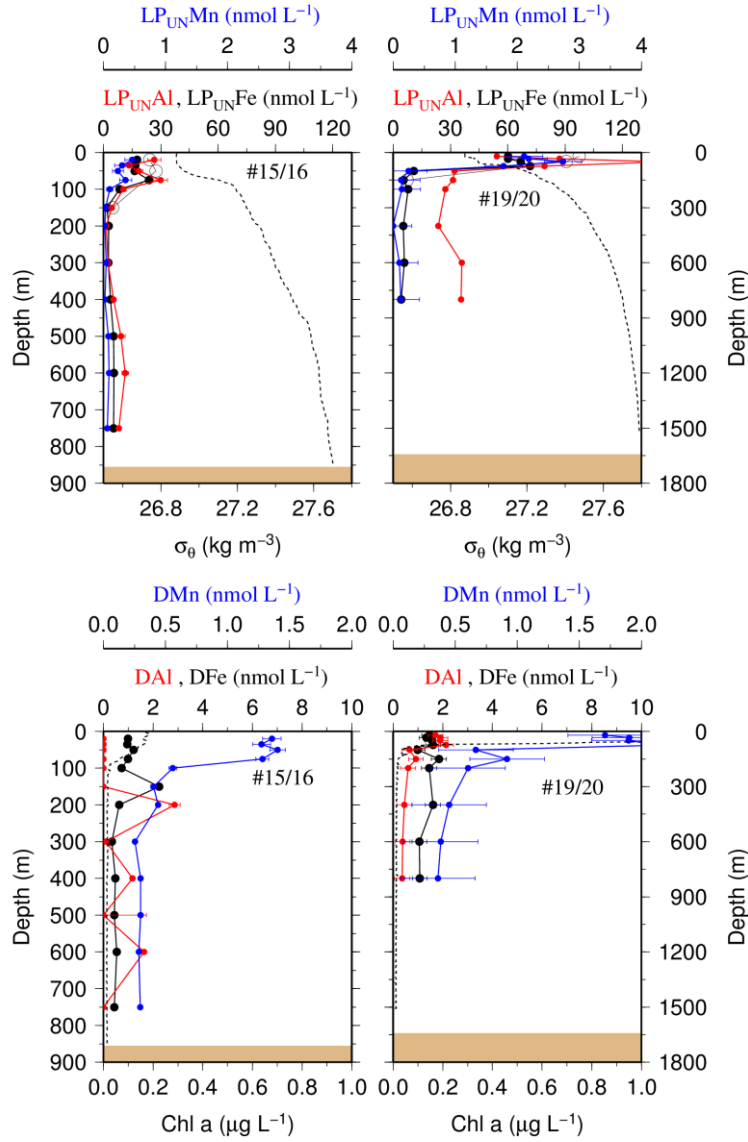each water column station (blue) and sediment core (brown) station to the nearest shore.

974

Figure 5: (Upper row) **OTE-seawater samples:** Distribution of leachable particulate

manganese (LP$_{Un}$Mn in blue), iron (LP$_{Un}$Fe in black), and aluminium (LP$_{Un}$Al in red)

concentrations in the water column of the two other stations located on the island shelf edge

(> 700 m water depth). **SAPS samples:** The particulate Fe (PFe) is illustrated by black circles

and corresponds to the concentration labels of LP$_{Un}$Fe. Error bars represent the standard

deviation of the analysis. Sigma-theta (σ_θ) is illustrated by the black dashed line. (Lower row)

OTE-seawater samples: Dissolved manganese (DMn), iron (DFe), and aluminium (DAl) are

represented by the same colour code as for the upper row. Dashed line illustrates the Chl a

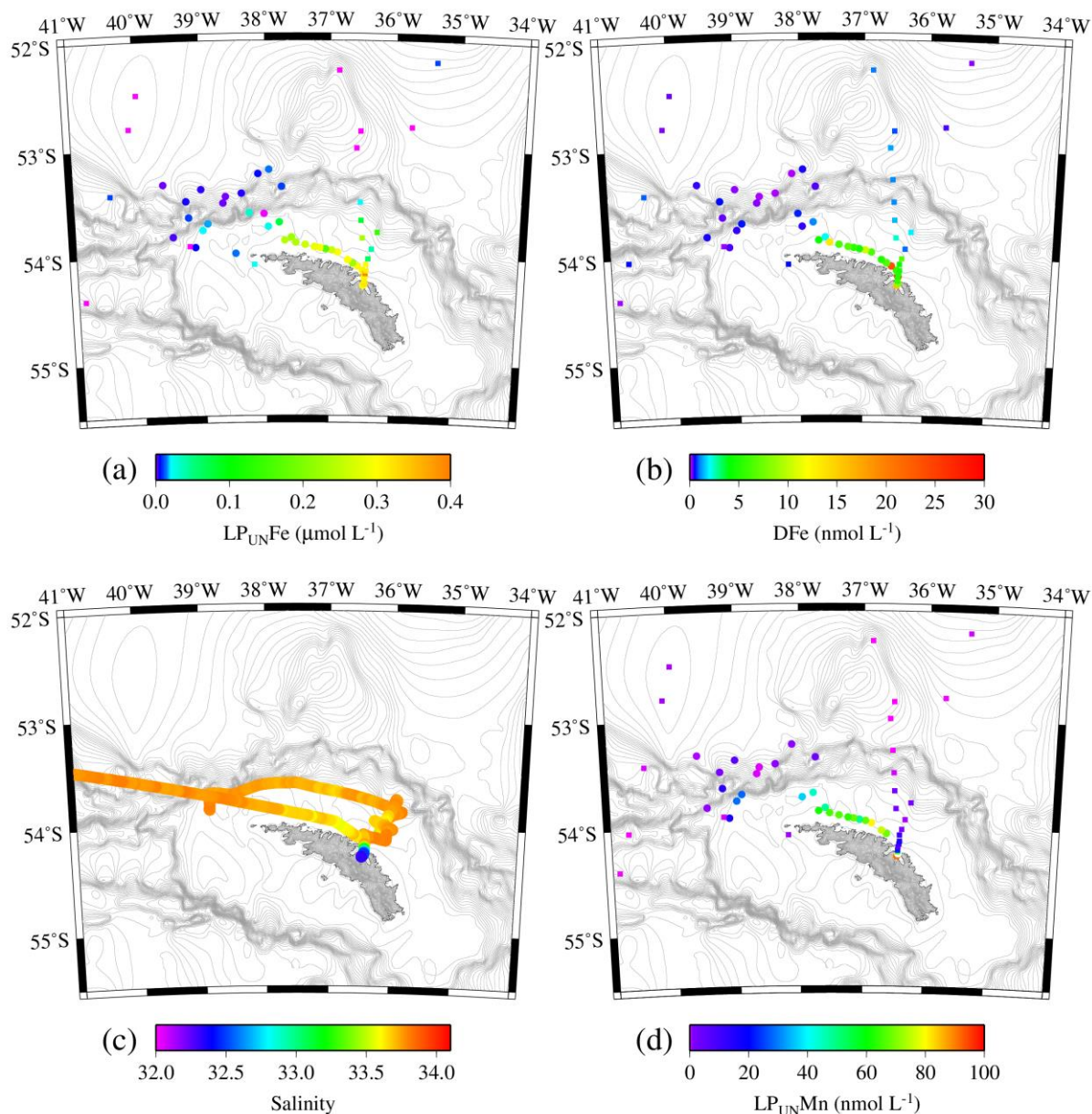content of the water column recorded by the CTD mounted fluorometer.

51

984

Figure 6: Tow fish-seawater samples: Concentrations of leachable particulate Fe (LP$_{UN}$Fe) of unfiltered seawater samples (a), dissolved Fe (DFe) (b), Salinity (c) and leachable particulate Mn (LP$_{UN}$Mn) in unfiltered seawater samples (d) in surface waters collected during JR247 (circles) and JR274 (squares) around South Georgia. The highest LP$_{UN}$Fe concentration was recorded in a single sample in Cumberland Bay reaching 2.2 μmol L^{-1}. Because of generally lower concentrations we excluded this data point in panel (a). Isobath are represented by grey lines (GEBCO – Gridded Bathymetry Data).
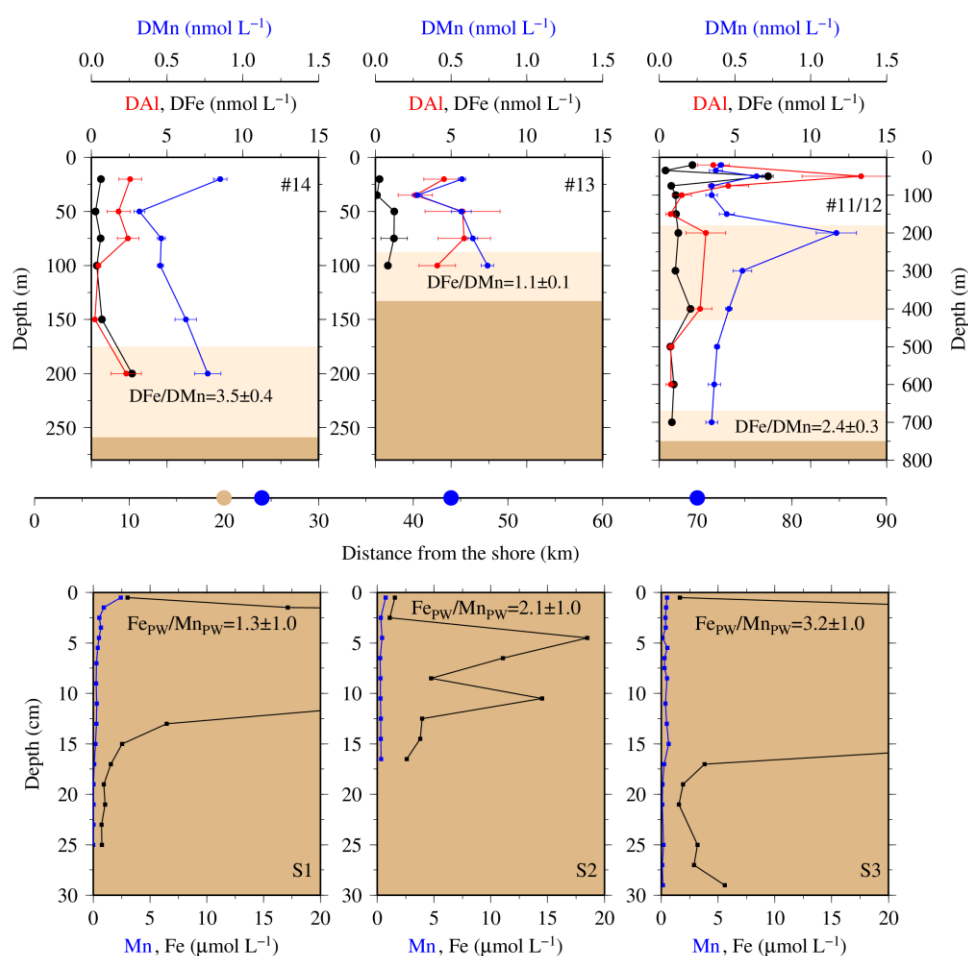
992

Figure 7: (Upper row) **OTE-seawater samples:** From left to right, concentrations of dissolved iron (DFe), aluminium (DAl), and manganese (DMn) for the two shelf sites (#14, #13) and the shelf edge site (#11/12). Note different depth scaling. Error bars represent the standard deviation of the analysis. Pink areas represent the zone of resuspended sediments in the water column. The DFe/DMn ratios of the seawaters collected within the pink zone is indicated. (Lower row) **Sediment core samples:** Diagram S1, S2 and, S3 displays the Fe (black), and Mn (blue) content in pore waters of the three sediment cores. Values off-axis can be found in Table 4. Shown are average Fe_{PW}/Mn_{PW} ratios (mol/mol) of top surface layer (1 cm) for site S1, S2, and S3. Dots on the distance scaling in the middle represent the distance of each water column station (blue) and sediment core (brown) station to the nearest shore.

DFe fluxes in µmol m^{-2} d^{-1}
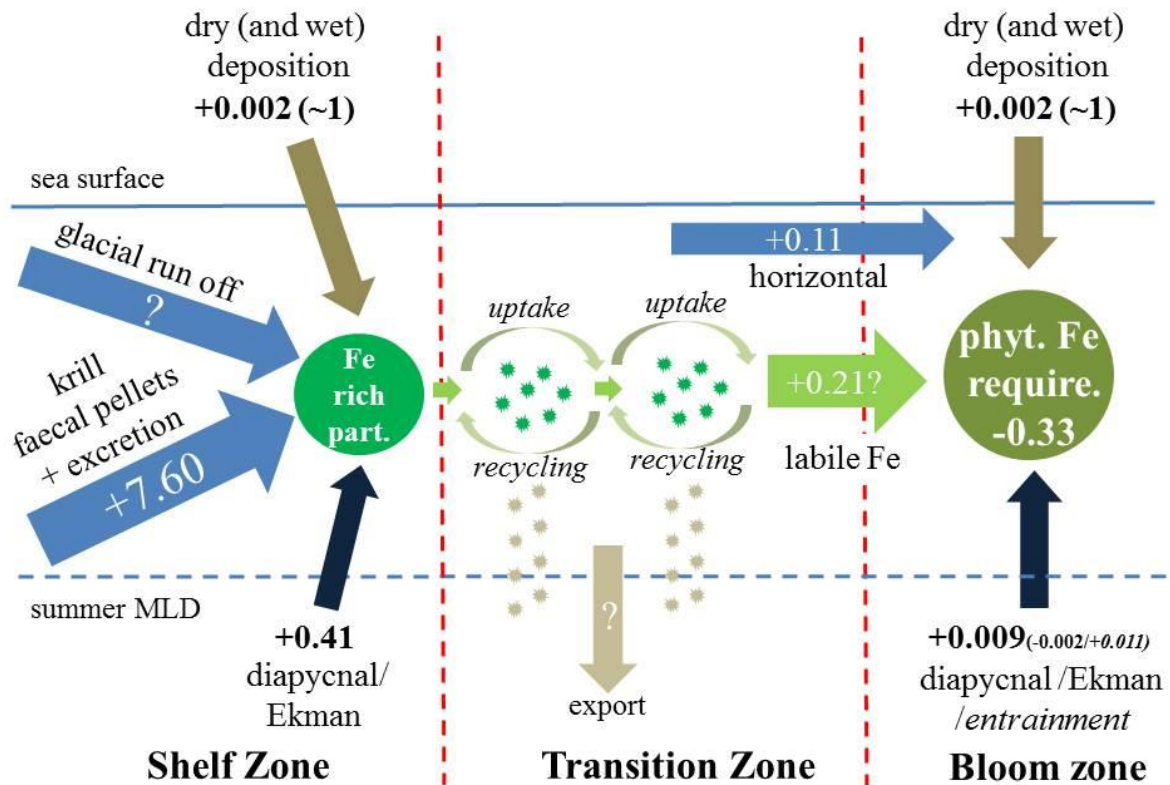
1004

1005 **Figure 8:** Sketch of DFe fluxes on the shelf, in the transition zone and in the downstream

1006 blooming region, separated by the red dashed lines. (left sketch) Describes the dissolved Fe

1007 fluxes on the shelf that together generate Fe rich biogenic and lithogenic particles (dark

1008 green). These are transferred offshore (light green arrows) following the ACC to open ocean

1009 sites (sketch in the middle). Iron enriched particles (dark green) in the transition zone are

1010 recycled and supplement DFe requirements of the phytoplankton community in the transition

1011 zone. During each cycle of recycling and uptake an unknown Fe fraction is lost by vertical

1012 export. (right sketch) Describes the dissolved Fe fluxes in the blooming zone.